Analysis of the operation of gradient echo memories using a quantum input–output model

2013 New J. Phys. 15 085020

(http://iopscience.iop.org/1367-2630/15/8/085020)

New Journal of Physics
The open access journal for physics

Analysis of the operation of gradient echo memories using a quantum input–output model

M R Hush[1,6], A R R Carvalho[3,4], M Hedges[5] and M R James[2,3]

[1] School of Physics and Astronomy, The University of Nottingham, Nottingham NG7 2RD, UK
[2] Research School of Engineering, The Australian National University, Canberra, ACT 0200, Australia
[3] ARC Centre for Quantum Computation and Communication Technology, The Australian National University, ACT 0200, Australia
[4] Department of Quantum Science, Research School of Physics and Engineering, The Australian National University, ACT 0200, Australia
[5] Institute for Quantum Science and Technology, University of Calgary, Calgary, Alberta T2N 1N4, Canada
E-mail: Michael.Hush@nottingham.ac.uk

New Journal of Physics **15** (2013) 085020 (33pp)
Received 8 May 2013
Published 22 August 2013
Online at http://www.njp.org/
doi:10.1088/1367-2630/15/8/085020

Abstract. The gradient echo memory (GEM) technique is a promising candidate for real devices due to its demonstrated performance, but to date high performance experiments can only be described numerically. In this paper we derive a model for GEM as a cascade of infinite interconnected harmonic oscillators. We take a quantum input–output approach to analyse this system, describing the read and write processes of GEM each as a linear-time-invariant process. We provide an analytical solution to the problem in terms of transfer functions which describe the memory behaviour for arbitrary inputs and operating regimes. This allows us to go beyond previous works and analyse the storage quality in the regimes of high optical depth and memory-bandwidth comparable to input bandwidth, exactly the regime of high-efficiency experiments.

[6] Author to whom any correspondence should be addressed.

Contents

1. Introduction

The creation of complex optical networks for quantum information is highly desirable for applications in secure communication and computing. In order to design these networks, not only high performance components will be required but highly accurate models of them. One of the most critical such components of is quantum memory. A theoretical model of the memories within a network will be necessary both to optimize individual devices and to compensate for remaining imperfections when many are chained together.

A quantum memory for light is a device that takes quantum information encoded onto an input pulse of light and maps it temporarily to a stationary, highly isolated medium. The information can be recalled as another pulse of light on-demand at a later time. The study

of quantum memory is a highly active field (see e.g. [1] and references therein). Practical implementation is complicated however by the competing requirements of weak decohering interactions with the environment but strong coupling to the desired light mode. Significant progress has been made by using large ensembles of identical atoms or ions each with a weak optical transition to get around this problem. While the interaction of a single absorber to both light and the environment is weak, the strength of coherent interaction with light scales with the number of absorbers squared [2].

A number memory of techniques using this ensemble approach have been investigated. Electromagnetically induced transparency has been the basis of many early investigations and demonstrations [3], while photon-echo type techniques such as controlled-reversible inhomogeneous broadening [4] and gradient echo memory (GEM) [5, 6], atomic frequency comb [7] and others [8–10] have received more recent attention. Techniques for producing quantum states within ensembles have also been explored [11, 12]. Stand-out demonstrations include storage of quantum states [13–17] and seconds long coherent storage [18] using electromagnetically induced transparency, highly efficient and non-conditional quantum storage with GEM [19–21], the delay of high-bandwidth entangled states with atomic frequency comb [22, 23], and the creation and storage of telecommunications wavelength photons in an optical lattice [24].

The technique known as GEM, or alternatively as a 'longitudinal' variant of controlled-reversible inhomogeneous broadening, is particularly promising for use in large scale networks. It has so far been the only technique demonstrated to perform as a quantum memory without requiring post-selection. It is also well suited to long-term storage on spin states [25, 26] and includes the ability to perform basic processing in-memory [27].

In addition to experimental studies, GEM has received significant theoretical attention. These efforts involved solving the Maxwell–Bloch equations in the linear, and slowly varying envelope approximations. Analytical and numerical studies performed in this area include the discussion of the basic principles of quantum memories [10, 28], multi-mode capacity [29, 30] and spectro-temporal mode distortions when the memory is optically thick [28, 29, 31]. Further generalizations to strong input fields and Raman transitons have also been considered [10, 26].

However, as yet, no exact solution has been shown for the behaviour of the basic memory, except in the limit where the memory bandwidth is much larger than that of the incoming pulse. This a significant impediment to the analysis of quantum memories, since, ideally, one should aim to maximize the memory performance by storing as much as possible within the memory bandwidth, i.e. two working in the regime where memory and input bandwidths are comparable.

In this paper we present a fully quantum mechanical description of the GEM based on a quantum input–output model [32]. The input and output channels provide a means for transmitting quantum states between network components [32–35], making our model suitable to be integrated into the design of more complex quantum networks. We provide an analytical solution for this model which is valid in all bandwidth and storage time regimes. This enables the investigation of the temporal distortions on the retrieved pulse which has been found to limit the memory fidelity in numerical studies [29, 31].

The paper is organized as follows. In section 2, we describe the model and its connections with previous GEM descriptions. We also derive the dynamical equations and discuss their formal solution. In section 3, we describe the write and read stages of the memory operation, present the full analytical solution in the time domain, and investigate the memory performance. Section 4 discusses the memory operation in different regimes and approximations. A frequency

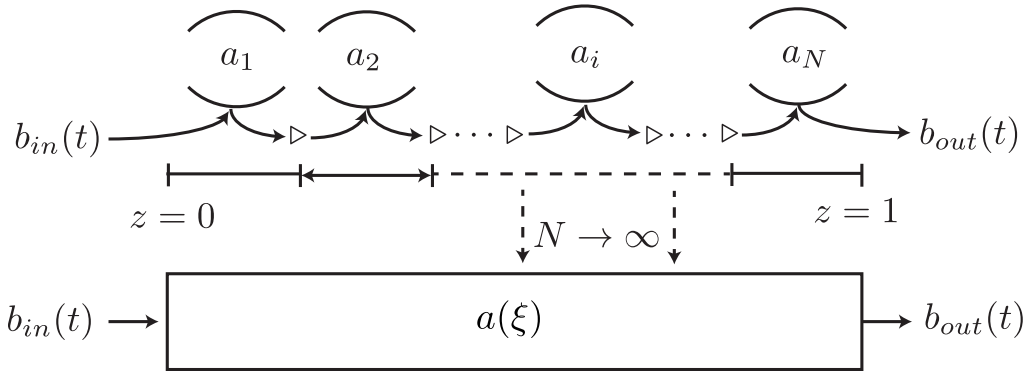

Figure 1. A cascade of cavities is used to represent the quantum memory. Light enters at left, passes through each cavity in term and then exits at right. A representation of the continuum GEM input–output model is shown at the bottom of the figure.

domain analysis is presented in section 5, providing a complementary perspective and further insight into the memory operation. We finally conclude with discussions and perspectives in section 6.

2. A network of oscillators as a model for a gradient echo quantum memory

Physically we may think of a GEM as a section of a material through which light is passed as shown in figure 1 (bottom). Incoming light, containing the quantum state to be stored, enters at the left and interacts with an ensemble of two-level atoms distributed within the material [6]. As a result of this interaction, the state of the light is stored in the medium. During this writing process a field gradient is applied to the material, producing a spatially selective storage of the different frequency components of the input signal. To read out the data, the gradient is reversed and the light emerges at the right.

In our model, the material is divided into slices (much smaller than the total memory length), each containing a large number of two-level atoms. We further consider the weak atomic excitation limit, a common regime in most experiments with GEM. This assumption allows us to replace the atomic operator algebra by that of harmonic oscillator operators [36], and hence to model each slice of material as a cavity. The full memory is modelled as a cascade network of cavities (oscillators) as the one shown in figure 1. In this section we will present an input–output model as a continuum limit of the cascade network and derive the corresponding dynamical equations in section 2.2. These are shown to be the quantum operator equations that lead to the Maxwell–Bloch equations in [28] and therefore our full quantum model represents faithfully the dynamics of GEM in the weak atomic excitation regime.

2.1. Derivation of the model

We consider a series of cavities connected as a cascade network as shown in figure 1. The cavities, described by the annihilation operators a_k, are coupled to the bosonic field b in such a way that the output of the cavity k is the input of cavity $k+1$. There are N cavities each one

with a slightly larger resonant frequency than the last due to the linear gradient applied. The kth cavity has resonant frequency $\xi_k = \eta(2k/N - 1)$. Thus the lowest frequency of the cavities is $-\eta$ and the highest is η. The input field $b_{\text{in}}(t)$ enters the system from the left, and, after interacting with the cavities, eventually emerges on the right side of the network as the output field $b_{\text{out}}(t)$.

To establish the relation between the input and output fields we will use the approach developed in [35] that describes the interconnection between Markovian open quantum systems forming a network. Each individual element of the network is described by the triple $G = (S, L, H)$, where S is a unitary corresponding to photon scattering (as in a phase shifter or beam splitter, for example), L describes the coupling between the system and the bosonic field, while H is the Hamiltonian of the system. In our model we have a set of elements connected in series, which corresponds to a cascade quantum system as studied in quantum optics [32, 33, 37]. In this case, each cavity is represented by the parameters

$$G_k = (I, \sqrt{\beta}\, a_k, \xi_k a_k^\dagger a_k). \tag{1}$$

Here, β is a dimensionless coupling constant between the cavities, while $a_k^\dagger$ and a_k are, respectively, the creation and annihilation operators for the kth cavity which obey the commutation relations $[a_j, a_k^\dagger] = \delta_{jk}$. The sign of the energy term $\xi_k a_k^\dagger a_k$ depends on the sign of the gradient and will be positive for the write stage, and negative for the read stage. We can weave these cavities together using the series product [35]. Explicitly connecting two elements G_1 and G_2 (with $S_1 = S_2 = I$) results in a Markovian model with parameters

$$G_1 \triangleright G_2 = \left(I, L_2 + L_1, H_1 + H_2 + \frac{1}{2\mathrm{i}}\left(L_2^\dagger L_1 - L_1^\dagger L_2\right)\right). \tag{2}$$

For a cascade of N elements, as shown in figure 1, we need to apply this rule $N - 1$ times to obtain

$$\begin{aligned} G &= G_1 \triangleright G_2 \triangleright \cdots G_i \cdots \triangleright G_N \\ &= \left(I, \sum_k L_k, \sum_k H_k + \frac{1}{2i}\sum_{j=2}^{N}\sum_{k}^{j-1}\left(L_j^\dagger L_k - L_k^\dagger L_j\right)\right). \\ &= \left(I, \mathrm{i}\sum_k \sqrt{\beta} a_k, \pm\sum_k \xi_k a_k^\dagger a_k + \frac{\beta}{2\mathrm{i}}\sum_{j=2}^{N}\sum_{k}^{j-1}\left(a_j^\dagger a_k - a_k^\dagger a_j\right)\right). \end{aligned} \tag{3}$$

We now take the continuous limit corresponding to $N \to \infty$ such that $\xi_i \to \xi \in (-\eta, \eta)$. In this limit the system is described by

$$\begin{aligned} G = \Bigg(I, \int_{-\eta}^{\eta} \mathrm{d}\xi\, \mathrm{i}\sqrt{\beta} a(\xi), \pm\int_{-\eta}^{\eta} \mathrm{d}\xi\, \xi a^\dagger(\xi) a(\xi) \\ + \frac{1}{2\mathrm{i}}\int_{-\eta}^{\eta}\mathrm{d}\xi \int_{-\eta}^{\eta}\mathrm{d}\xi'\, \beta\left(a^\dagger(\xi)a(\xi') - a^\dagger(\xi')a(\xi)\right)\Bigg), \end{aligned} \tag{4}$$

where $a(\xi)$ is the continuous version of the annihilation operator satisfying the commutation relation $[a(\xi), a^\dagger(\xi')] = \delta(\xi - \xi')$, and we assumed an equal coupling constant β for all the cavities. The parameter η describes the endpoints of the detuning interval $\xi \in [-\eta, \eta]$ corresponding to the GEM model in figure 1. Since there is a one-to-one correspondence between the position z and the detuning ξ, throughout the paper we will refer to ξ as detuning or spatial variable.

2.2. Dynamics: quantum Langevin equations

The quantum Langevin equation for an arbitrary operator X in an input–output model is given by [32]

$$\partial_t X = -\mathrm{i}[X, H] + \mathcal{D}^*[L]X + b_{\mathrm{in}}^\dagger(t)[X, L] - [X, L^\dagger]b_{\mathrm{in}}(t), \tag{5}$$

where $\mathcal{D}^*[L]X = \frac{1}{2}(L^\dagger[X, L] - [X, L^\dagger]L)$ and $b_{\mathrm{in}}(t)$ is the input light field. The output field is given by

$$b_{\mathrm{out}}(t) = L(t)\,\mathrm{d}t + b_{\mathrm{in}}(t). \tag{6}$$

Using the parameters equation (4) for the GEM model in equation (5) one can straightforwardly write the equation for $X = a(\xi)$ as

$$\partial_t a(\xi, t) = \mp\mathrm{i}\xi a(\xi, t) - \beta \int_{-\eta}^{\xi} \mathrm{d}\xi'\, a(\xi', t) + \mathrm{i}\sqrt{\beta}\, b_{\mathrm{in}}(t). \tag{7}$$

The corresponding output equation is

$$b_{\mathrm{out}}(t) = \mathrm{i}\sqrt{\beta} \int_{-\eta}^{\eta} \mathrm{d}\xi'\, a(\xi', t) + b_{\mathrm{in}}(t). \tag{8}$$

Now, if we define the operator

$$b(\xi, t) = \mathrm{i}\sqrt{\beta} \int_{-\eta}^{\xi} \mathrm{d}\xi' a(\xi', t) + b_{\mathrm{in}}(t), \tag{9}$$

we can write the dynamical equations for the GEM model in the form

$$\partial_t a(\xi, t) = \mp\mathrm{i}\xi a(\xi, t) + \mathrm{i}\sqrt{\beta} b(\xi, t), \tag{10}$$

$$\partial_\xi b(\xi, t) = \mathrm{i}\sqrt{\beta} a(\xi, t). \tag{11}$$

The input and output operators now act as boundary conditions for the equation (11), specifically $b_{\mathrm{in}}(t) = b(-\eta, t)$ and $b_{\mathrm{out}}(t) = b(\eta, t)$.

The dynamical equations (10) and (11) are fully quantum mechanical equations relating the input and output field operators to the internal mode operators. These equations have similar form to the Maxwell–Bloch equations for GEM, equations (3) and (4) in [28]. Note that with minor changes we can also model other memory schemes such as the one based on rephasing amplified spontaneous emission, for example.

2.3. Formal solution of the gradient echo memory equations

In order to understand the functioning of a quantum memory, we need to analyse the output of the memory in response to an arbitrary input signal. This is a familiar scenario in many areas of engineering such as control theory and signal processing, where the common approach is to use the concept of *linear time-invariant (LTI) systems* [38]. Even though the memory as a whole does not fit in this category (because of the change of gradient), the individual write and read stages of the memory do. If we think of $a(\xi, t)$ as a vector of infinite dimension, $a(t)$, then the memory equations (7) and (8) can be expressed into the LTI form

$$\dot{a}(t) = Aa(t) + Bb_{\mathrm{in}}(t), \tag{12}$$

$$b_{\mathrm{out}}(t) = Ca(t) + Db_{\mathrm{in}}(t). \tag{13}$$

The linear operators (infinite 'matrices') A, B, C and D act on a vector v as $[Mv](\xi) = \int_{-\eta}^{\eta} \mathrm{d}\xi' M(\xi,\xi')v(\xi')$, and are given in component form by $A_{\xi,\xi'} = \mp \mathrm{i}\xi\delta(\xi-\xi') + \beta\Theta(\xi-\xi')$, $B_{\xi,1} = \mathrm{i}\sqrt{\beta}$, $C_{1,\xi} = \mathrm{i}\sqrt{\beta}$, and $D_{1,1} = 1$, with $\Theta(\cdot)$ being the Heaviside step function. The operators A, B and C satisfy the identities

$$A + A^\dagger + C^\dagger C = 0, \tag{14}$$

$$B = -C^\dagger. \tag{15}$$

The general solution for the quantum mechanical operators $a(t)$ and $b_{\mathrm{out}}(t)$ can be obtained by formally integrating the LTI equations (12) and (13) (with $D = 1$):

$$a(t) = \mathrm{e}^{At}a(0) + \int_0^t \mathrm{e}^{A(t-r)}Bb_{\mathrm{in}}(r)\mathrm{d}r, \tag{16}$$

$$b_{\mathrm{out}}(t) = C\,\mathrm{e}^{At}a(0) + \int_0^t C\,\mathrm{e}^{A(t-r)}Bb_{\mathrm{in}}(r)\mathrm{d}r + b_{\mathrm{in}}(t). \tag{17}$$

Explicit expressions for these fundamental transfer relations will be given in sections 3.2 and 3.3 in the time domain, and in sections 5.1 and 5.2 for the frequency domain.

2.4. Energy balance

The quantum mechanical GEM equations (12) and (13) (or (16) and (17) in integrated form) contain important physical information regarding energy flows and energy storage in the quantum memory. The energy (quanta) balance equations presented in this section will be used in subsequent sections to help us understand the operation of the quantum memory.

The GEM number operator

$$n(t) = \int_{-\eta}^{\eta} a^\dagger(\xi,t)a(\xi,t)\,\mathrm{d}\xi = a^\dagger(t)a(t) \tag{18}$$

describes the number of quanta stored within the memory at time t, and is related to the input and output field number operators

$$\Lambda_{\mathrm{in}}(t) = \int_0^t b_{\mathrm{in}}^\dagger(r)b_{\mathrm{in}}(r)\,\mathrm{d}r \quad \text{and} \quad \Lambda_{\mathrm{out}}(t) = \int_0^t b_{\mathrm{out}}^\dagger(r)b_{\mathrm{out}}(r)\,\mathrm{d}r, \tag{19}$$

respectively, by the energy balance identity

$$\Lambda_{\mathrm{out}}(t) + n(t) = \Lambda_{\mathrm{in}}(t) + n(0). \tag{20}$$

The operators $\Lambda_{\mathrm{in}}(t)$ and $\Lambda_{\mathrm{out}}(t)$ count, respectively, the number of incoming and outgoing quanta up to time t. The operator (Heisenberg picture) equation (20), which can be derived using stochastic calculus [32], says that at any time $t \geqslant 0$ the sum of the total incoming quanta and the initial quanta must be equal to the amount of quanta that has flowed out plus the quanta that have been stored.

2.5. Quantum states

Since the purpose of a quantum memory is to store and retrieve quantum information, in this section we discuss precisely what this means and explain how the Heisenberg picture GEM equations (12) and (13) (or (16) and (17)) may be used to understand the quantum memory operation.

The dynamical evolution of the GEM system and field is governed by a unitary $U(t)$ [32, 39], so that, for example, $a(\xi, t) = U^\dagger(t)a(\xi, 0)U(t)$. The state of the system and field is given by the Schrödinger picture evolution

$$|\Psi(t)\rangle = U(t)|\Psi_{\text{GEM}}\rangle \otimes |\Psi_{\text{field}}\rangle, \tag{21}$$

where $|\Psi_{\text{GEM}}\rangle$ is the initial GEM state and $|\Psi_{\text{field}}\rangle$ is the field state. This shows that the GEM system and field are in a joint state $|\Psi(t)\rangle$ at time t, and the reduced states for either the GEM system or the field may be obtained by the appropriate partial traces.

It is often easier to consider moments rather than states. For instance, if the GEM system is initially in the vacuum state $|\Psi_{\text{GEM}}\rangle = |0\rangle$ and if the input field is in a coherent state $|\Psi_{\text{field}}\rangle = |\beta_{\text{in}}\rangle$ (where $\beta_{\text{in}}(\cdot)$ is a complex function of time), then moments may easily be evaluated. The means $\alpha(t) = \langle a(t)\rangle$, $\beta_{\text{in}}(t) = \langle b_{\text{in}}(t)\rangle$ and $\beta_{\text{out}}(t) = \langle b_{\text{out}}(t)\rangle$ are related by the *envelope equations*

$$\alpha(t) = \int_0^t \mathrm{e}^{A(t-r)} B \beta_{\text{in}}(r)\, \mathrm{d}r, \tag{22}$$

$$\beta_{\text{out}}(t) = \int_0^t C\, \mathrm{e}^{A(t-r)} B \beta_{\text{in}}(r) \mathrm{d}r + \beta_{\text{in}}(t), \tag{23}$$

while the mean GEM photon number $\bar{n}(t) = \langle n(t)\rangle$ is related to the mean field intensities $\bar{\Lambda}_{\text{in}}(t) = \langle \Lambda_{\text{in}}(t)\rangle$ and $\bar{\Lambda}_{\text{out}}(t) = \langle \Lambda_{\text{out}}(t)\rangle$ by

$$\bar{\Lambda}_{\text{out}}(t) + \bar{n}(t) = \bar{\Lambda}_{\text{in}}(t) \tag{24}$$

using (20). The terms in equation (24) may be expressed in terms of $\alpha(t)$, $\beta_{\text{in}}(t)$ and $\beta_{\text{out}}(t)$ as follows:

$$\int_0^t |\beta_{\text{out}}(r)|^2\, \mathrm{d}r + |\alpha(t)|^2 = \int_0^t |\beta_{\text{in}}(r)|^2\, \mathrm{d}r. \tag{25}$$

In particular, note that the mean internal stored energy at time t is given by

$$\bar{n}(t) = |\alpha(t)|^2 = \int_{-\eta}^{\eta} |\alpha(\xi, t)|^2\, \mathrm{d}\xi. \tag{26}$$

As another example, suppose instead that the field is initially in a single photon state $|\Psi_{\text{field}}\rangle = \int_0^\infty \beta_{\text{in}}(r) b_{\text{in}}^\dagger(r)\, \mathrm{d}r |0_{\text{field}}\rangle$, where $\beta_{\text{in}}(\cdot)$ is a wavepacket pulse shape satisfying $\int_0^\infty |\beta_{\text{in}}(r)|^2\, \mathrm{d}r = 1$. Then the energy balance equation (25) continues to hold, with $\alpha(t)$ and $\beta_{\text{out}}(t)$ again given by equations (22) and (23), respectively. In this single photon driving case, however, the envelopes $\alpha(t)$ and $\beta_{\text{out}}(t)$ are no longer the mean values—the means are instead zero.

We see therefore that the infinite matrix quantities $\mathrm{e}^{At}B$, $C\,\mathrm{e}^{At}B$, (and also $C\,\mathrm{e}^{At}$ for including initial condition terms) determine the moments of the GEM model (system and field operators). In the forthcoming sections we will focus on obtaining and analysing these functions

for the write and read stages of the memory. In order to do so, we find it convenient to define $\beta(\xi,t) = \mathrm{i}\sqrt{\beta}\int_{-\eta}^{\xi} \mathrm{d}\xi' \alpha(\xi',t) + \beta_{\mathrm{in}}(t)$ (as in equation (9)), and write the envelope equations in the form

$$\partial_t \alpha(\xi,t) = \mp \mathrm{i}\xi\alpha(\xi,t) + \mathrm{i}\sqrt{\beta}\beta(\xi,t), \tag{27}$$

$$\partial_\xi \beta(\xi,t) = \mathrm{i}\sqrt{\beta}\alpha(\xi,t). \tag{28}$$

3. Quantum memory operation: exact analysis in the time domain

3.1. Stages of operation

The operation of a quantum memory is usually described in two stages: a write stage where information contained in the input light is mapped to the internal degrees of the memory, and a read stage where the information is retrieved to produce the output signal. Figure 2 shows a schematic of these two stages. In the write phase the gradient is on until $t = T$ and an input pulse $\beta^{\mathrm{in}}_{\mathrm{write}}$ with width ϵ_t is stored as atomic excitation in the memory ($\alpha^{\mathrm{out}}_{\mathrm{write}}$). In this stage, the memory has no excitations to start with ($\alpha(\xi,0) = 0$, vacuum internal state in figure 2(b), and $\beta^{\mathrm{out}}_{\mathrm{write}}$ represents the light that passes straight through the memory, corresponding to inefficiencies in the process. At the end of this phase at time $t = T$, the gradient is flipped and the memory outputs until $t = 2T$ a time reversed version of the input pulse. In the read stage, the excitation is initially stored in the memory as $\alpha^{\mathrm{in}}_{\mathrm{read}} = \alpha^{\mathrm{out}}_{\mathrm{write}}$ and is output as a light field $\beta^{\mathrm{out}}_{\mathrm{read}}$. There is no incoming light field during this phase (vacuum input in figure 2(c)) and any excitation remaining in the memory ($\alpha^{\mathrm{out}}_{\mathrm{read}}$) corresponds to inefficiencies in the read stage.

3.2. Write stage transfer equations

For the write stage, we set the gradient to a negative value, so that the 'matrix' A in the GEM model, section 2.3, is given by

$$A_{\xi,\xi'} = -\mathrm{i}\xi\delta(\xi-\xi') + \beta\Theta(\xi-\xi'). \tag{29}$$

During the write stage, there is no initial excitation stored in the memory and in response to the driving input, we employ the envelope equations corresponding to (22) and (23) in the form

$$\alpha^{\mathrm{out}}_{\mathrm{write}}(\xi) = \int_0^T h_{\mathrm{write}}(\xi, T-r)\beta_{\mathrm{in}}(r)\,\mathrm{d}r, \tag{30}$$

$$\beta^{\mathrm{out}}_{\mathrm{write}}(t) = \int_0^t g_{\mathrm{write}}(t-r)\beta_{\mathrm{in}}(r)\,\mathrm{d}r, \tag{31}$$

where we have used the initial condition $\alpha(\xi,0) = 0$, the definition $\alpha^{\mathrm{out}}_{\mathrm{write}}(\xi) = \alpha(\xi,T)$, and included the dependence on the detuning variable ξ explicitly. The solutions for the impulse responses h_{write} and g_{write}, derived in detail in appendix A.1, are given by

$$h_{\mathrm{write}}(\xi,t) = [\mathrm{e}^{At}B]_{\xi,1} = \mathrm{i}\sqrt{\beta}\,\mathrm{e}^{-\mathrm{i}\xi t}L\left(-\mathrm{i}\beta, \mathrm{i}t(\xi+\eta)\right), \tag{32a}$$

$$g_{\mathrm{write}}(t) = C\,\mathrm{e}^{At}B + \delta(t) = -2\beta\eta\,\mathrm{e}^{-\mathrm{i}\eta t}\,{}_1F_1\left(1+\mathrm{i}\beta, 2, 2\mathrm{i}\eta t\right) + \delta(t), \tag{32b}$$

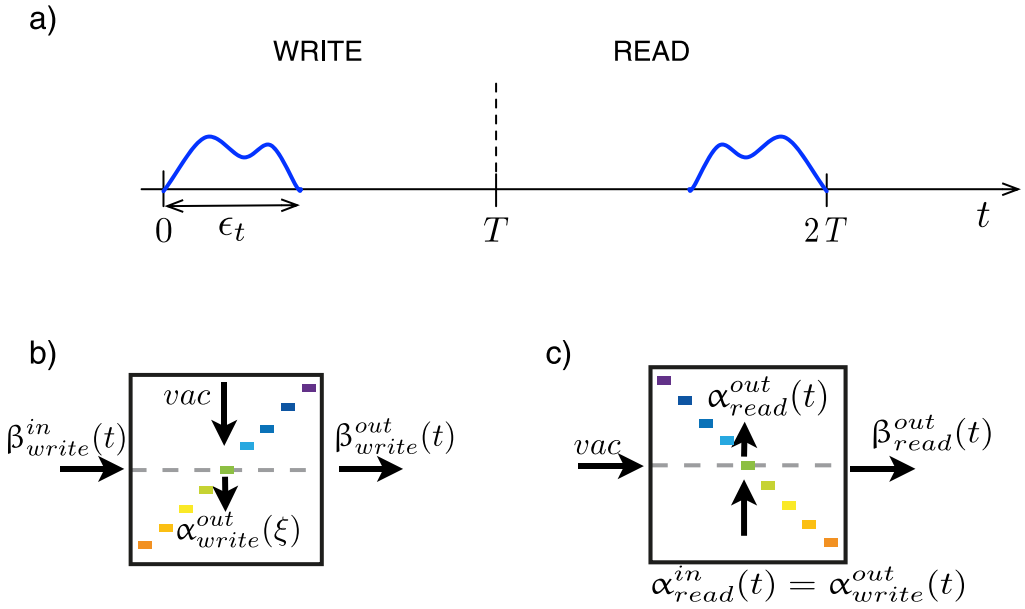

Figure 2. Write and read stages. (a) Typical time domain envelope waveforms, showing the input signal and the final output signal, which appears reversed in time and subject to distortion. (b), (c) Illustration of the gradients applied in each stage, as well as a representation of the initialization and inputs for each stage.

where $L(n, x)$ is a Laguerre function and ${}_1F_1(a, b, x)$ is a Kummer confluent hypergeometric function as defined in appendix B. Equations (32*a*) and (32*b*) are the main analytical expressions for the write phase in the time domain and contains all the necessary ingredients to obtain the storage behaviour of the memory in any operating regime and for any input field.

3.3. Read stage transfer equations

For the read stage, we change the gradient from the positive value used in the write stage to a negative value. The 'matrix' A in the GEM model, section 2.3, is given by

$$A_{\xi,\xi'} = +\mathrm{i}\xi\,\delta(\xi - \xi') + \beta\Theta(\xi - \xi'). \tag{33}$$

In the scenario depicted in figure 2, we assume that the read stage occurs on an interval $T < t < 2T$ after the write stage. The initial condition for the read stage is then given by the value of the atomic excitation at the end of the write process ($t = T$). In this case, the envelope equations (22) and (23) can be solved as

$$\alpha(t) = \mathrm{e}^{A(t-T)}\alpha^{\mathrm{in}}_{\mathrm{read}}, \tag{34}$$

$$\beta(t) = C\,\mathrm{e}^{A(t-T)}\alpha^{\mathrm{in}}_{\mathrm{read}}, \tag{35}$$

where $\alpha^{\mathrm{in}}_{\mathrm{read}} = \alpha^{\mathrm{out}}_{\mathrm{write}}$ and $\beta^{\mathrm{in}}_{\mathrm{read}} = 0$. Write $\beta^{\mathrm{out}}_{\mathrm{read}}(t) = \beta(t)$ for $T < t < 2T$ and, on setting $t = 2T$, write $\alpha^{\mathrm{out}}_{\mathrm{read}}(\xi) = \alpha(\xi, 2T)$. These output quantities may be expressed as follows:

$$\alpha^{\mathrm{out}}_{\mathrm{read}}(\xi) = \int_{-\eta}^{\xi} h_{\mathrm{read}}(\xi - \xi')\alpha^{\mathrm{in}}_{\mathrm{read}}(\xi')\,\mathrm{d}\xi', \tag{36}$$

$$\beta^{\text{out}}_{\text{read}}(t) = \int_{-\eta}^{\eta} g_{\text{read}}(\xi', t - T)\alpha^{\text{in}}_{\text{read}}(\xi')\,\mathrm{d}\xi', \tag{37}$$

where $T < t < 2T$, and

$$h_{\text{read}}(\xi) = -T\beta \mathrm{e}^{-\mathrm{i}T\xi}\,{}_1F_1\,(1 + \mathrm{i}\beta, 2, \mathrm{i}T\xi) + \delta(\xi), \tag{38}$$

$$g_{\text{read}}(\xi, t') = \mathrm{i}\sqrt{\beta}\,\mathrm{e}^{\mathrm{i}\xi t'} L\left(-\mathrm{i}\beta, it'(\eta - \xi)\right) \tag{39}$$

for $t' \geqslant 0$. For details on how these solutions were derived see appendix A.2.

Note the symmetry between these results and the ones obtained in the write stage. The stored excitation as well as the memory output are both given in terms of the impulse responses containing the Laguerre functions while the inefficiency terms, i.e. the light that is not stored and the excitation that remains in the memory after the recall, are both governed by the responses with the hypergeometric function.

3.4. Adjusting the time variable

As shown in figure 2(a), the output of the GEM after the write and read stages is reversed in time and subject to distortion. In order to assess the quality of the GEM, it is helpful if we adjust the time variable so that the input and output signals can more easily be compared. In addition, the analysis to follow will be simpler if time and frequency are put on similar footings.

To this end we set $\tau = T/2$ and for the write stage we shift time to the left by τ units, i.e. we define $\breve{\beta}_{\text{in}}(t) = \beta_{\text{in}}(t + \tau)$ and $\breve{\alpha}(\xi, t) = \alpha(\xi, t + \tau)$ for $-\tau \leqslant t \leqslant \tau$. Then $\alpha^{\text{out}}_{\text{write}}(\xi) = \breve{\alpha}(\xi, \tau)$. Next, define $\breve{\beta}_{\text{out}}(t) = \beta_{\text{out}}(-t + 2T - \tau)$. Finally dropping the $\breve{\cdot}$ notation, the write stage equations (30) and (31) become

$$\alpha^{\text{out}}_{\text{write}}(\xi) = \int_{-\tau}^{\tau} h_{\text{write}}(\xi, \tau - r)\beta_{\text{in}}(r)\,\mathrm{d}r, \tag{40}$$

$$\beta^{\text{out}}_{\text{write}}(t) = \int_{-\tau}^{t} g_{\text{write}}(t - r)\beta_{\text{in}}(r)\,\mathrm{d}r, \tag{41}$$

while the read equation (37) becomes

$$\beta^{\text{out}}_{\text{read}}(t) = \int_{-\eta}^{\eta} g_{\text{read}}(\xi', -t + \tau)\alpha^{\text{in}}_{\text{read}}(\xi')\,\mathrm{d}\xi'. \tag{42}$$

All signals β_{in}, $\beta^{\text{out}}_{\text{write}}$ and $\beta^{\text{out}}_{\text{read}}$ are understood to be defined on the time interval $[-\tau, \tau]$. In particular, $\beta_{\text{in}}(t)$ and $\beta^{\text{out}}_{\text{read}}(t)$ are directly comparable for $t \in [-\tau, \tau]$.

3.5. Memory performance from the exact solution

With the solutions for the write and read stage at hand, we are now in a position to investigate the overall performance of the memory. The simple energy balance relations discussed in section 2.4

suggest a measure of efficiency comparing input and output energies. For the write stage, we have

$$\int_{-\tau}^{\tau} |\beta_{\text{write}}^{\text{out}}(t)|^2 \, \mathrm{d}t + \int_{-\eta}^{\eta} |\alpha_{\text{write}}^{\text{out}}(\xi)|^2 \, \mathrm{d}\xi = \int_{-\tau}^{\tau} |\beta_{\text{write}}^{\text{in}}(t)|^2 \, \mathrm{d}t, \tag{43}$$

where

$$E_{\text{write}}^{\text{store}} = \int_{-\eta}^{\eta} |\alpha_{\text{write}}^{\text{out}}(\xi)|^2 \, \mathrm{d}\xi \tag{44}$$

is the energy stored within the memory, and

$$E_{\text{write}}^{\text{in}} = \int_{-\tau}^{\tau} |\beta_{\text{write}}^{\text{in}}(t)|^2 \, \mathrm{d}t \tag{45}$$

is the energy input to the memory during the write stage. For the read stage we have

$$\int_{-\tau}^{\tau} |\beta_{\text{read}}^{\text{out}}(t)|^2 \, \mathrm{d}t + \int_{-\eta}^{\eta} |\alpha_{\text{read}}^{\text{out}}(\xi)|^2 \, \mathrm{d}\xi = \int_{-\eta}^{\eta} |\alpha_{\text{read}}^{\text{in}}(\xi)|^2 \, \mathrm{d}\xi, \tag{46}$$

where

$$E_{\text{read}}^{\text{out}} = \int_{-\tau}^{\tau} |\beta_{\text{read}}^{\text{out}}(t)|^2 \, \mathrm{d}t \tag{47}$$

is the energy output from the memory during the read stage. Since $\alpha_{\text{read}}^{\text{in}} = \alpha_{\text{write}}^{\text{out}}$, we may combine these expressions to give

$$\int_{-\tau}^{\tau} |\beta_{\text{read}}^{\text{out}}(t)|^2 \, \mathrm{d}t = \int_{-\tau}^{\tau} |\beta_{\text{write}}^{\text{in}}(t)|^2 \, \mathrm{d}t - \ell, \tag{48}$$

where the total write–read *loss* is defined by

$$\ell = \int_{-\tau}^{\tau} |\beta_{\text{write}}^{\text{out}}(t)|^2 \, \mathrm{d}t + \int_{-\eta}^{\eta} |\alpha_{\text{read}}^{\text{out}}(\xi)|^2 \, \mathrm{d}\xi. \tag{49}$$

The *efficiency* is defined by

$$\mathcal{E} = \frac{\int_{-\infty}^{\infty} |\beta_{\text{read}}^{\text{out}}(t)|^2 \, \mathrm{d}t}{\int_{-\infty}^{\infty} |\beta_{\text{write}}^{\text{in}}(t)|^2 \, \mathrm{d}t}, \tag{50}$$

where we have allowed for an extension of the range of integration if necessary. In view of the non-negative loss ℓ, we have that $\mathcal{E} \leqslant 1$, and so a quantum memory with $\mathcal{E}$ as close to 1 as possible is desirable, since this corresponds to high energy transfer through the memory.

Efficiency is primarily a statement about the total energy stored and retrieved by the memory. However, for a high-performance quantum memory, not only the intensity but also the phase of the input signal must be reconstructed accurately. To quantify how well the phase information is reproduced, we use the *overlap* between the $\beta_{\text{read}}^{\text{out}}(t)$ and $\beta_{\text{write}}^{\text{in}}(t)$ defined as

$$\mathcal{O} = \frac{|\int_{-\infty}^{\infty} (\beta_{\text{read}}^{\text{out}}(t))^* \beta_{\text{write}}^{\text{in}}(t) \, \mathrm{d}t|^2}{\int_{-\infty}^{\infty} |\beta_{\text{read}}^{\text{out}}(t)|^2 \, \mathrm{d}t \int_{-\infty}^{\infty} |\beta_{\text{write}}^{\text{in}}(t)|^2 \, \mathrm{d}t}. \tag{51}$$

The overlap lies strictly in the interval $0 \leqslant \mathcal{O} \leqslant 1$ and when $\mathcal{O} = 1$ we can be certain that $\beta_{\text{read}}^{\text{out}}(t)/\sqrt{\int_{-\infty}^{\infty} |\beta_{\text{read}}^{\text{out}}(t')|^2 \, \mathrm{d}t'} = \beta_{\text{write}}^{\text{in}}(t)/\sqrt{\int_{-\infty}^{\infty} |\beta_{\text{write}}^{\text{in}}(t')|^2 \, \mathrm{d}t'}$, assuming $\beta_{\text{read}}^{\text{out}}(t)$, $\beta_{\text{write}}^{\text{in}}(t) \in L_2$. Overlap is in some sense independent of efficiency as a signal can have $\mathcal{O} = 1$

but $\mathcal{E} \neq 1$ and vice versa. A quantum memory can only be considered perfect when both $\mathcal{O} = 1$ *and* $\mathcal{E} = 1$ in which case we can prove $\beta^{\text{out}}_{\text{read}}(t) = \beta^{\text{in}}_{\text{write}}(t)$ (up to an absolute phase factor). Thus maximizing both the efficiency, $\mathcal{E}$, and overlap, $\mathcal{O}$, is key to creating a high performance quantum memory.

We now use the exact transfer equations to analyse the efficiency and overlap for the GEM. The results are shown in figure 3. We assumed an initial Gaussian input pulse described by the variances σ_τ and σ_η in time and frequency, respectively. The memory performance will depend on how well this input pulse fits the memory characteristics. For this reason, the important quantities to be considered are the ratios between the memory bandwidth η and σ_η, and the writing time τ and σ_τ. In figure 3(a) we plot the efficiency as a function of these ratios. Figures 3(c), (e) and (d) show cross-sections of figures 3(a) and (b) for fixed values of τ, η and the product $\tau\eta$, respectively. We see that the more the pulse fits in the memory bandwidth and storage time, the more efficient the memory becomes. This is consistent with previous analysis of GEM in the broadband limit [28]. What is important to note here is that our analytical solution allows us to probe the inefficiencies of the memory in regions of parameters previously only accessible through numerical simulations.

The efficiency is not the only measure that must be maximized, overlap is important as well. The overlap, depicted in figure 3(b), is consistently lower than the efficiency. It only gets close to one for very large bandwidths and storage times and typically lags behind the efficiency. This demonstrates that the memory has caused a phase mismatch between the input and output pulse.

We emphasize at this point that, although it is important to maximize both overlap and efficiency, a low overlap is typically much easier to correct for than a low efficiency. To correct for a low efficiency the output signal would need to be amplified, if performed deterministically this process would irreversibly introduce extra noise into the signal. A low overlap on the other hand is due to a mismatch of phase. As long as this phase mismatch can be characterized accurately it can be corrected for deterministically without the addition of any extra noise to the system.

Characterization of this phase mismatch can be achieved using the analytic solution we have provided. At the moment this phase mismatch looks like it could depend on precisely what input signal was received. This would make correcting it very difficult if not impossible. Fortunately we will find that in many relevant limits the phase change by the GEM is *independent* of the input signal. Making it much easier to correct for.

4. Quantum memory operation: approximate analysis in the time domain

Even though our exact analytical solutions allowed us to give a complete picture of the memory performance as shown in figure 3, at first they look too complicated to provide any insight about the physics underlying GEM. In this section, however, we will revisit our solutions for the write and read stages to show that they can be used to understand the basic principles of quantum memories, their limitations, the different working regimes and the approximations behind them.

4.1. Basic assumptions

Now we will consider that the input pulse is limited in both time and frequency such that

$$\beta^{\text{in}}_{\text{write}}(t) \approx 0 \quad \text{when } t < -\epsilon_\tau \text{ or } t > \epsilon_\tau \tag{52}$$

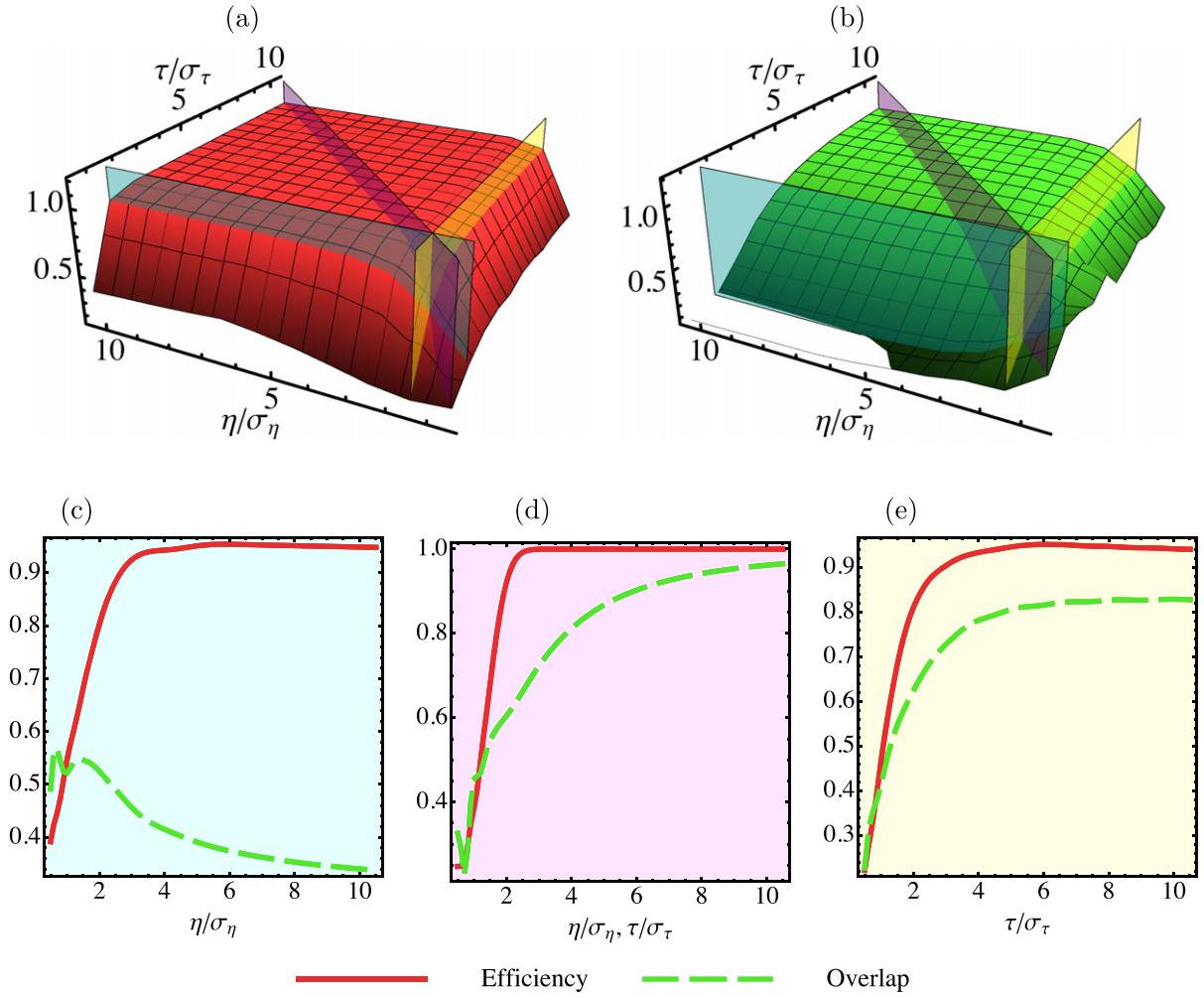

Figure 3. Performance of the GEM under two different measures: (a) efficiency and (b) overlap. The data was produced by calculating $\beta^{\text{out}}_{\text{read}}(t)$ directly from equations (37) and (30), (32*a*) with $\beta = 2$ and a Gaussian initial condition for the input field ($\beta^{\text{in}}_{\text{write}}(t) = A\pi^{-1/4}\exp(-t^2/2\sigma_\tau^2)$). The horizontal axes show the storage time and frequency bandwidth normalized with respect to the variances of the input pulse in time (σ_τ) and in frequency ($\sigma_\eta = 1/\sigma_\tau$). The semi-transparent planes in (a) and (b) correspond to the cross-sections presented in (c)–(e). In (c), τ/σ_τ is kept fixed and η/σ_η is increased, in (d) η/σ_η and τ/σ_τ are scaled at the same rate and in (e) η/σ_η is kept fixed and τ/σ_τ is increased. The efficiency saturates to its maximum value once $\eta/\sigma_\eta > \epsilon_\eta/\sigma_\eta \approx 3$ or $\tau/\sigma_\tau > \epsilon_\tau/\sigma_\tau \approx 3$, agreeing with the prediction that efficiency will be very close to $(1 - \mathrm{e}^{-2\pi\beta})^2$ when the signal fits within the time and frequency window of the memory (see section 4). The overlap, on the other hand, lags behind considerably if the memory operates outside the broadband and long storage time limits.

and

$$\tilde{\beta}^{\text{in}}_{\text{write}}(\omega) \approx 0 \quad \text{when } \omega < -\epsilon_\eta \text{ or } \omega > \epsilon_\eta. \tag{53}$$

We will also make the assumption

$$|(\tau - \epsilon_\tau)(\eta - \epsilon_\eta)| \gg 1 \tag{54}$$

which allows us to approximate the Laguerre functions, as detailed in appendix C, to obtain, for the write stage,

$$\alpha^{\text{out}}_{\text{write}}(\xi) = \chi(\beta) \int_{-\tau}^{\tau} \mathrm{d}t\, \mathrm{e}^{-\mathrm{i}\xi(\tau-t)-\mathrm{i}\beta\ln(\tau-t)(\eta+\xi)} \beta^{\text{in}}_{\text{write}}(t). \tag{55}$$

Here $\chi(\beta) = \mathrm{i}\frac{\sqrt{\beta}\,\mathrm{e}^{-\pi\beta/2}}{\Gamma(1-\mathrm{i}\beta)}$ and therefore

$$|\chi(\beta)|^2 = \frac{1-\mathrm{e}^{-2\pi\beta}}{2\pi}. \tag{56}$$

Looking closely to equation (55), we can see that the term $\mathrm{e}^{-\mathrm{i}\xi(\tau-t)}$, that would correspond to a Fourier transform, is accompanied by a logarithm term that produces a nonlinear time and frequency dependent phase shift. This factor complicates the analysis but is also the key signature that our solution goes beyond the broadband approximation.

For the read stage, under assumption (54) we can approximate the solution as

$$\beta^{\text{out}}_{\text{read}}(t) = \chi(\beta) \int_{-\eta}^{\eta} \mathrm{d}\xi\, \mathrm{e}^{\mathrm{i}\xi(\tau-t)-\mathrm{i}\beta\ln(\tau-t)(\eta-\xi)} \alpha^{\text{in}}_{\text{read}}(\xi). \tag{57}$$

We see again the logarithm term alongside a Fourier-like term. This time, however, we also have the memory bandwidth governing how close to a Fourier transform this term actually is.

4.2. *Efficiency*

We now use the approximations introduced in the previous section to estimate the efficiency $\mathcal{E}$. To begin the analysis, let us look at the total excitation stored in the material, $E^{\text{store}}_{\text{write}}$ defined by (44). This is given by

$$E^{\text{store}}_{\text{write}} = |\chi(\beta)|^2 \int_{-\eta}^{\eta} \mathrm{d}\xi \int_{-\tau}^{\tau} \mathrm{d}t' \int_{-\tau}^{\tau} \mathrm{d}t\, \mathrm{e}^{-\mathrm{i}\xi(t'-t)-\mathrm{i}\beta\ln\left(\frac{(\tau-t')}{(\tau-t)}\right)} \beta^{\text{in}}_{\text{write}}(t')^* \beta^{\text{in}}_{\text{write}}(t). \tag{58}$$

In view of assumptions (52) and (53) we can extend the limits in the integrals to infinity to obtain

$$E^{\text{store}}_{\text{write}} \approx (1-\mathrm{e}^{-2\pi\beta}) E^{\text{in}}_{\text{write}}. \tag{59}$$

In this approximation, the effect of the phase factor is simply to add a windowing effect: the memory absorbs in the window of the time it was stored, attenuated by the factor $2\pi|\chi(\beta)|^2$.

Next, the total output energy is given by

$$\begin{aligned} E^{\text{out}}_{\text{read}} &= \int_{-\infty}^{\infty} \mathrm{d}t' |\beta^{\text{out}}_{\text{read}}(t')|^2 \approx \int_{-\tau}^{\tau} \mathrm{d}t' |\beta^{\text{out}}_{\text{read}}(t')|^2 \\ &= |\chi(\beta)|^2 \int_{-\tau}^{\tau} \mathrm{d}t' \int_{-\eta}^{\eta} \mathrm{d}\xi' \int_{-\eta}^{\eta} \mathrm{d}\xi\, \mathrm{e}^{\mathrm{i}(\tau-t')(\xi'-\xi)-\mathrm{i}\beta\ln\left(\frac{(\eta-\xi')}{(\eta-\xi)}\right)} \alpha^{\text{in}}_{\text{read}}{}^{\dagger}(\xi) \alpha^{\text{in}}_{\text{read}}(\xi') \\ &= 2\pi|\chi(\beta)|^2 \int_{-\eta}^{\eta} \mathrm{d}\xi\, |\alpha^{\text{in}}_{\text{read}}(\xi)|^2 \\ &= 2\pi|\chi(\beta)|^2 E^{\text{store}}_{\text{write}}, \end{aligned} \tag{60}$$

where in the first line we assumed that the output signal fits within the writing time window, equation (52). Note that we do not necessarily assume that the input signal is stored in a much larger time than its width in time. We see that the excitation of the system will come out with the same attenuation factor as before. Now, If we use assumption (53) that the input and output pulses fit within the bandwidth of the memory we find

$$E^{\text{out}}_{\text{read}} \approx (1 - \mathrm{e}^{-2\pi\beta})^2 E^{\text{in}}_{\text{write}}. \tag{61}$$

Consequently we find that the efficiency is given approximately by

$$\mathcal{E} \approx (1 - \mathrm{e}^{-2\pi\beta})^2. \tag{62}$$

We should emphasize that this is only valid when the input and output pulses fit well within the bandwidth of the system. Otherwise, the system will filter out parts of the input pulse that lie outside its bandwidth (this is discussed further in section 5.1 below).

4.3. Long write limit

We now make the stronger assumption that the write time is much larger than the pulse width

$$\tau \gg \epsilon_\tau. \tag{63}$$

This assumption will allow us to understand the operation of the GEM in the long write regime.

4.3.1. Write stage. Under the long write assumption (63) we can approximate the logarithm by $\ln(\tau - t) \approx \ln \tau$ and write the our solution (55) as

$$\alpha^{\text{out}}_{\text{write}}(\xi) = \chi(\beta) \int_{-\tau}^{\tau} \mathrm{d}t' \, \mathrm{e}^{-\mathrm{i}\xi(\tau - t') - \mathrm{i}\beta \ln \tau(\eta + \xi)} \beta^{\text{in}}_{\text{write}}(t'). \tag{64}$$

Since $\tau \gg \epsilon_\tau$, we can extend the limits of the integral to infinity and obtain

$$\alpha^{\text{out}}_{\text{write}}(\xi) = \chi(\beta) \, \mathrm{e}^{-\mathrm{i}\xi\tau - \mathrm{i}\beta \ln \tau(\eta + \xi)} \hat{\beta}^{\text{in}}_{\text{write}}(-\xi), \tag{65}$$

where

$$\hat{\beta}^{\text{in}}_{\text{write}}(\xi) = \int_{-\infty}^{\infty} \mathrm{e}^{-\mathrm{i}\xi r} \beta^{\text{in}}_{\text{write}}(r) \, \mathrm{d}r \tag{66}$$

is the Fourier transform of the input. Thus we can see that the excitation in the medium will have the shape of the Fourier transform of the input pulse within the memory bandwidth. Note again that $-\eta < \xi < \eta$ so frequencies outside of this bandwidth will of course simply pass through the memory in the long term.

Equation (65) shows that the Fourier transform of the input is subject to attenuation and phase distortion. The attenuation (magnitude) is given by the constant factor

$$M^{\text{long write}}_{\text{write}} = |\chi(\beta)| = \sqrt{\frac{1 - \mathrm{e}^{-2\pi\beta}}{2\pi}} \tag{67}$$

which is consistent with the energy transfer relation (59). The phase distortion is a logarithmic function of the spatial variable ξ:

$$\phi^{\text{long write}}_{\text{write}}(\xi) = -\xi\tau - \beta \ln \tau(\eta + \xi). \tag{68}$$

Figure 4 shows the full transfer function as a function of the write time determined from the exact solution (32*a*). For large write times, the magnitude and phase of the transfer approach the approximate values given by equations (67) and (68).

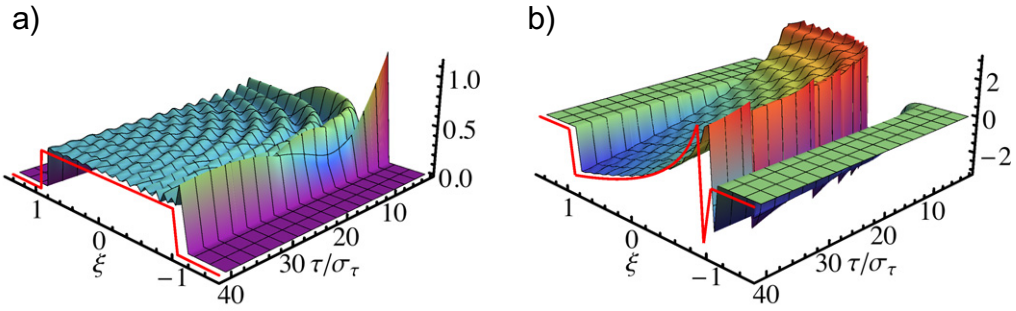

Figure 4. An example of the exact solution of the GEM during write stage approaching the approximate transfer function with attenuation (67) (a) and phase distortion (68) (b). The transfunction interpretation of what is stored and read from the memory is only appropriate in approximate limits so a direct comparison with the exact solution is not technically possible. However we can still gain a great deal of intuition by examining what is stored in the memory, $\alpha^{\text{in}}_{\text{write}}$, given an delta function input pulse, $\beta^{\text{in}}_{\text{write}}(t) = \delta(t)$. As the time stored becomes longer, $\alpha^{\text{in}}_{\text{write}}$ will approach the transfer functions: as the transform of a $\delta(t)$ function is flat, our output is essentially the transfer functions times 1. We can see that both the absolute value of $\alpha^{\text{in}}_{\text{write}}$ (a) and the argument of $\alpha^{\text{in}}_{\text{write}}$ (b) approach the expected approximated values in the long time limit. Note that in (b) we subtracted a constant phase across the frequencies, $\eta\tau$, to both the exact and approximate limits to make the detail in the plots clearer.

4.3.2. Read stage. The read phase in the limit of long storage times is given by

$$\beta^{\text{out}}_{\text{read}}(t) = \chi(\beta) \int_{-\eta}^{\eta} \mathrm{d}\xi \, \mathrm{e}^{\mathrm{i}\xi(\tau - t) - \mathrm{i}\beta \ln \tau(\eta - \xi)} \alpha^{\text{in}}_{\text{read}}(\xi). \tag{69}$$

We saw in the write stage that even though the excitation in the memory was simply related to the Fourier transform of the input pulse, because the system will only absorb frequencies within its bandwidth, the output pulse will not necessarily recreate the input pulse perfectly in time. To analyse the output pulse, let us look at it in Fourier space. For $-\eta < \xi < \eta$, we have

$$\begin{aligned}\hat{\beta}^{\text{out}}_{\text{read}}(\xi) &= 2\pi\chi(\beta) \int_{-\eta}^{\eta} \mathrm{d}\xi' \delta(\xi' + \xi) \, \mathrm{e}^{\mathrm{i}\tau\xi' - \mathrm{i}\beta \ln \tau(\eta - \xi)} \alpha^{\text{in}}_{\text{read}}(\xi') \\ &= 2\pi\chi(\beta) \, \mathrm{e}^{\mathrm{i}\tau\xi - \mathrm{i}\beta \ln \tau(\eta - \xi)} \alpha^{\text{in}}_{\text{read}}(-\xi). \end{aligned} \tag{70}$$

This equation displays the attenuation and phase distortion during the read phase. Explicitly, the attenuation (magnitude) of the read transfer is given by

$$M^{\text{long write}}_{\text{read}} = 2\pi \sqrt{\frac{1 - \mathrm{e}^{-2\pi\beta}}{2\pi}} \tag{71}$$

and the corresponding phase is

$$\phi^{\text{long write}}_{\text{read}}(\xi) = \tau\xi - \beta \ln \tau(\eta - \xi). \tag{72}$$

This result is essentially the same as for the write stage, with just with a change of signs in the ξ terms in the phase response corresponding to the gradient flip.

Note that these results apply for $-\eta < \xi < \eta$, the detuning range of the GEM. Within this range, equation (70) says that in Fourier ξ-space, the output equals the internal storage up to attenuation and phase distortion factors. If we were to define ξ outside the spatial range of the GEM, then equation (70) would give $\tilde{\beta}^{\text{out}}_{\text{read}}(\xi) = 0$, corresponding to a window effect in the Fourier domain.

4.3.3. The whole memory process: write and read stages combined. We can now combine both stages and analyse the full memory cycle. The total attenuation and phase distortion may be obtained by combining the contributions from the write and read stages:

$$\begin{aligned} M^{\text{long write}}_{\text{write–read}} &= M^{\text{long write}}_{\text{write}} M^{\text{long write}}_{\text{read}} \\ &= 2\pi |\chi(\beta)|^2 = 1 - \mathrm{e}^{-2\pi\beta} \end{aligned} \tag{73}$$

and

$$\begin{aligned} \phi^{\text{long write}}_{\text{write–read}}(\xi) &= \phi^{\text{long write}}_{\text{write}}(\xi) + \phi^{\text{long write}}_{\text{read}}(\xi) \\ &= -2\beta \ln \tau(\eta+\xi)(\eta-\xi). \end{aligned} \tag{74}$$

This can be seen from (70) and (65)

$$\begin{aligned} \hat{\beta}^{\text{out}}_{\text{read}}(\xi) &= \chi(\beta)\, \mathrm{e}^{\mathrm{i}\xi(\tau-t)-\mathrm{i}\beta \ln \tau(\eta-\xi)} \hat{\alpha}^{\text{in}}_{\text{read}}(-\xi) \\ &= \chi(\beta)^2\, \mathrm{e}^{\mathrm{i}\xi(\tau-t)-\mathrm{i}\beta \ln \tau(\eta-\xi)}\, \mathrm{e}^{-\mathrm{i}\xi\tau-\mathrm{i}\beta \ln \tau(\eta+\xi)} \hat{\beta}^{\text{in}}_{\text{write}}(\xi) \\ &= 2\pi\chi(\beta)^2\, \mathrm{e}^{-\mathrm{i}2\beta \ln \tau(\eta+\xi)(\eta-\xi)} \hat{\beta}^{\text{in}}_{\text{write}}(-\xi). \end{aligned} \tag{75}$$

This equation is valid only between $-\eta < \xi < \eta$, outside this region $\hat{\beta}^{\text{out}}_{\text{read}}(\xi) = 0$. The output emerging from the write–read cycle in the *freqency domain* approximately equals the input up to attenuation and phase distortion factors. In the time domain the input and output fields may not necessarily match well.

To investigate the validity of these approximations, we look again at the exact solution. We have shown that in the limit of long storage time the power spectrum of the output field is the same as in the input field within the bandwidth of the memory. Both the efficiency and overlap have stronger requirements than just this to achieve a value of 1, so neither are good indicators of the approximations we have applied in this chapter being valid. So we now introduce a new measure, the *frequency domain shape overlap (FDSO)*,

$$\mathcal{O}_\omega = \frac{|\int_{-\infty}^{\infty} \mathrm{d}\omega |\hat{\beta}^{\text{out}}_{\text{read}}(\omega)\| \hat{\beta}^{\text{in}}_{\text{write}}(\omega)\|^2}{\int_{-\infty}^{\infty} \mathrm{d}\omega |\hat{\beta}^{\text{out}}_{\text{read}}(\omega)|^2 \int_{-\infty}^{\infty} \mathrm{d}\omega |\hat{\beta}^{\text{in}}_{\text{write}}(\omega)|^2}, \tag{76}$$

This measures how well the shape of the power spectra of the input and output fields match. It is easy to show that when we replace our approximate solution, equation (75), into equation (76) we get $\mathcal{O}_\omega = 1$. Figure 5(a) shows $\mathcal{O}_\omega$ calculated from the exact solution as a function of the writing time and bandwidth for the same set of parameters of figure 3. The growth of the FDSO in figure 5(e) confirms that the results we have derived in this section are valid in the long storage time limit.

4.4. Broadband limit

In order to study the behaviour of a broadband memory, in place of assumption (63) we now assume

$$\eta \gg \epsilon_\eta, \tag{77}$$

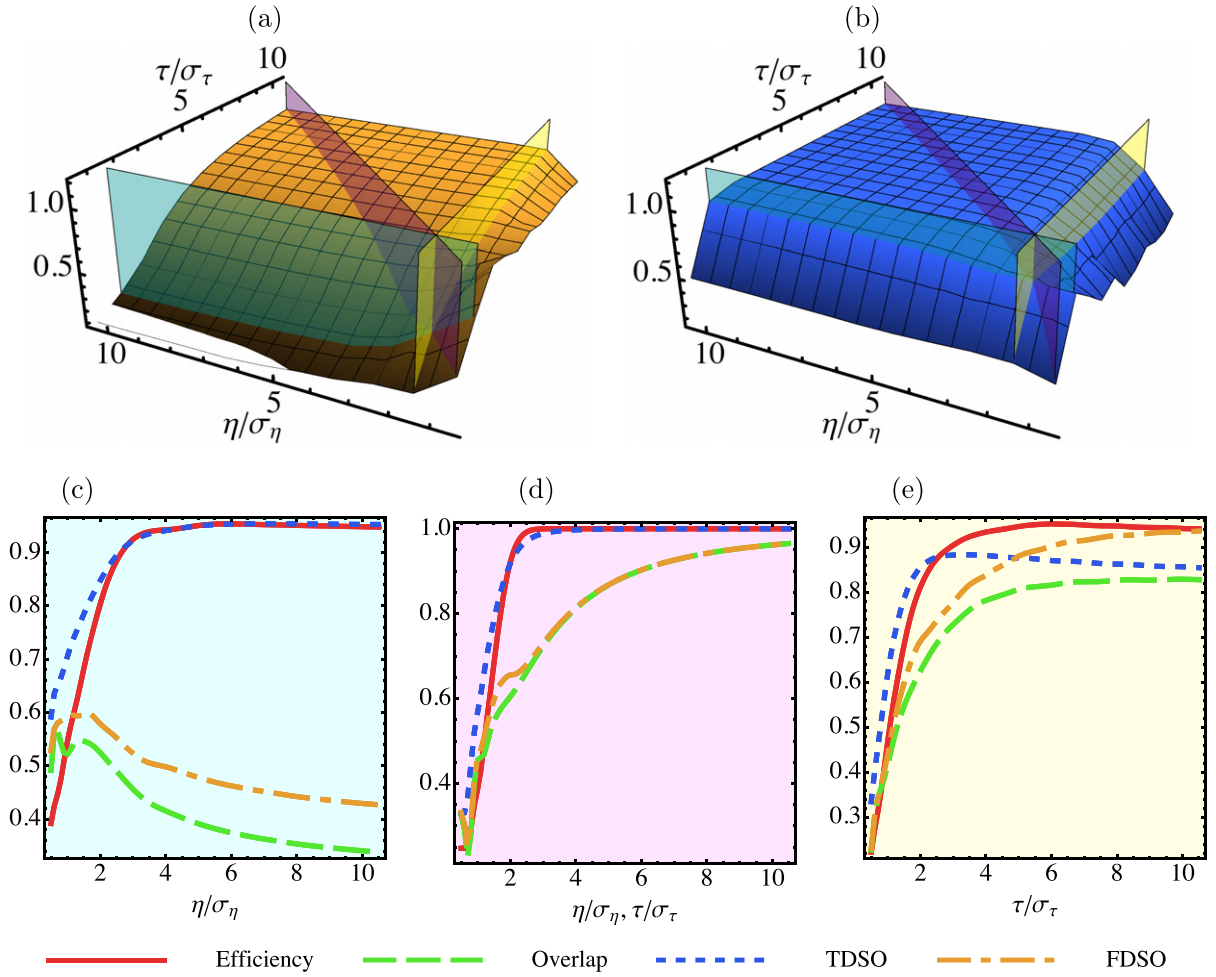

Figure 5. Time domain shape overlap (TDSO) (a) and FDSO for the same set of parameters of figure 3. The cross-sections in (c)–(e) also show the efficiency and overlap curves from figure 3 for comparison. The TDSO improves very quickly in the broadband limit, essentially matching the efficiency when $\eta/\sigma_\eta > \epsilon_\eta/\sigma_\eta \approx 3$. Its dual, the FDSO, does not improve much the in broadband limit and only benefits from long storage times as shown in (g). In fact in this limit it actually improves beyond the TDSO. Ultimately the overlap is not maximized unless both the TDSO and FDSO are both high, this only occurs in (f) when both τ/σ_τ and η/σ_η are increased. Even though we have taken special care to ensure that the time and frequency domain are treated on an equal footing we see a clear asymmetry in the behaviour of the measures this is investigated in more detail in section 4.6.

which says that memory bandwidth is much larger than the width in frequency of input pulse. This is an important limit that will allow us to show how our general solution reduces to results previously investigated in the literature [28].

Under assumption (77) the equations for the envelopes become

$$\alpha^{\text{out}}_{\text{write}}(\xi) = \chi(\beta)\int_{-\tau}^{\tau} \mathrm{d}t\, \mathrm{e}^{-\mathrm{i}\xi(\tau-t)-\mathrm{i}\beta\ln(\tau-t)\eta}\beta^{\text{in}}_{\text{write}}(t), \tag{78}$$

$$\beta^{\text{out}}_{\text{read}}(t) = \chi(\beta)\int_{-\eta}^{\eta} \mathrm{d}\xi\, \mathrm{e}^{\mathrm{i}\xi(\tau-t)-\mathrm{i}\beta\ln(\tau-t)\eta}\alpha^{\text{in}}_{\text{read}}(\xi). \tag{79}$$

These are in agreement with the analysis performed by Longdell *et al* [28]. Note the similarity between these equations and (64) and (69). In our analysis we can clearly see that the long writing time approximation and the broadband one act as the dual of one another. This will be further emphasized as we look at the read and write stages.

4.4.1. Write stage. Because we are assuming the broadband limit but not necessarily the long writing time limit, it turns out that what is stored is not the Fourier transform of the input. This is due to the t dependent logarithmic term in equation (78). Nevertheless, we may take the inverse Fourier transform

$$\breve{\alpha}^{\text{out}}_{\text{write}}(t) = \frac{1}{2\pi}\int_{-\infty}^{\infty} \mathrm{e}^{\mathrm{i}\xi t}\alpha^{\text{out}}_{\text{write}}(\xi)\,\mathrm{d}\xi \tag{80}$$

to find that the overlap of the input pulse is of a high quality. Explicitly,

$$\begin{aligned}\breve{\alpha}^{\text{out}}_{\text{write}}(t) &= \chi(\beta)\int_{-\infty}^{\infty}\mathrm{d}\xi\int_{-\tau}^{\tau}\mathrm{d}t'\,\mathrm{e}^{-\mathrm{i}\xi(\tau-t'-t)-\mathrm{i}\beta\ln(\tau-t')\eta}\beta^{\text{in}}_{\text{write}}(t')\\ &= 2\pi\chi(\beta)\int_{-\tau}^{\tau}\mathrm{d}t'\delta(\tau-t'-t)\,\mathrm{e}^{-\mathrm{i}\beta\ln(\tau-t')\eta}\beta^{\text{in}}_{\text{write}}(t')\\ &= \begin{cases}2\pi\chi(\beta)\,\mathrm{e}^{-\mathrm{i}\beta\ln t\eta}\beta^{\text{in}}_{\text{write}}(\tau-t), & -\tau<t<\tau,\\ 0, & t<-\tau \text{ or } t>\tau\end{cases}.\end{aligned} \tag{81}$$

Consequently for $-\tau < t < \tau$ the transfer to the internal storage has attenuation (magnitude)

$$M^{\text{broadband}}_{\text{write}} = 2\pi|\chi(\beta)| = \sqrt{1-\mathrm{e}^{-2\pi\beta}} \tag{82}$$

and phase

$$\phi^{\text{broadband}}_{\text{write}} = -\beta\ln t\eta. \tag{83}$$

We see again the attenuation factor and a windowing effect similar to what we saw before. This time there is a window with regard to the input pulse time, rather than a frequency filter.

4.4.2. Read stage. Much like in the previous sections, we look at the attenuation and phase distortion. Under the broadband assumption we have

$$\beta^{\text{out}}_{\text{read}}(t) = \chi(\beta)\,\mathrm{e}^{-\mathrm{i}\beta\ln(\tau-t)\eta}\breve{\alpha}^{\text{in}}_{\text{read}}(\tau-t) \tag{84}$$

and so the attenuation and phase are given by

$$M^{\text{broadband}}_{\text{read}} = |\chi(\beta)| = \sqrt{\frac{1-\mathrm{e}^{-2\pi\beta}}{2\pi}} \tag{85}$$

and

$$\phi^{\text{broadband}}_{\text{read}}(\xi) = -\beta\ln(\tau-t)\eta. \tag{86}$$

These relations are valid inside the time window $-\tau < t < \tau$. We see that only the light input within the writing window will be stored and retrieved.

4.4.3. The whole memory process: write and read stages combined. We can now combine both stages and analyse the full memory cycle under the broadband assumption (77). Indeed, it follows immediately from equations (81) and (84) that

$$\beta^{\text{out}}_{\text{read}}(t) = 2\pi\,\chi(\beta)^2\,\mathrm{e}^{-\mathrm{i}2\beta\ln(\tau-t)\eta}\,\beta^{\text{in}}_{\text{write}}(t). \tag{87}$$

The total attenuation and phase distortion are given by

$$M^{\text{broadband}}_{\text{write–read}} = 2\pi\,|\chi(\beta)|^2 = 1-\mathrm{e}^{-2\pi\beta} \tag{88}$$

and

$$\phi^{\text{broadband}}_{\text{write–read}}(t) = -2\beta\ln(\tau-t)\eta. \tag{89}$$

We see that the output signal is identical to the input field up to the phase factor. The phase factor means that the same may not necessarily be true in the frequency domain. We see that the long time limit approximation and broadband approximation are the dual of one another. In the long storage time domain limit the power spectrum of input signal is accurately reproduced in the output signal within the bandwidth of the memory. In the broadband case the opposite occurs, instead the intensity over time is reproduced accurately within the storage time window of the memory.

We again use the exact solutions to investigate this approximation. We have shown that the intensity of the output field over time will perfectly match the intensity of the input field, up to an attenuation factor. Both the efficiency and overlap have stronger requirements than just this to achieve a value of 1, so neither are good indicators of the approximations we have applied in this section being valid. So we introduce a new measure the TDSO,

$$\mathcal{O}_t = \frac{|\int_{-\infty}^{\infty}\mathrm{d}t|\hat{\beta}^{\text{out}}_{\text{read}}(t)\parallel\hat{\beta}^{\text{in}}_{\text{write}}(t)\parallel^2}{\int_{-\infty}^{\infty}\mathrm{d}t|\hat{\beta}^{\text{out}}_{\text{read}}(t)|^2\int_{-\infty}^{\infty}\mathrm{d}t|\hat{\beta}^{\text{in}}_{\text{write}}(t)|^2}, \tag{90}$$

which gives a measure of how correct we get the shape of the output beam in the time domain. It is easy to show that when we replace our approximated solution, equation (87), into equation (90) we get $\mathcal{O}_t = 1$. The behaviour of the TDSO obtained from the analytical solution can be seen in figure 5(b) and the corresponding cross-sections in figures 5(c)–(e). The result in figure 5(c) shows a complementary behaviour of the TDSO as compared to FDSO: as we approach the broadband limit, the shape of the output signal improves but only does so in the *time* domain.

4.5. Broadband and long storage time approximations

Now we will consider the limit underlying most of the intuitive understanding of GEM described in the literature in terms of Fourier transform. If we consider both the long writing time and broadband limits, the time domain transfer functions reduce to

$$\alpha^{\text{out}}_{\text{write}}(\xi) = \chi(\beta)\,\mathrm{e}^{-\mathrm{i}\beta\ln\tau\eta}\int_{-\infty}^{\infty}\mathrm{d}t\,\mathrm{e}^{-\mathrm{i}\xi(\tau-t)}\beta^{\text{in}}_{\text{write}}(t), \tag{91}$$

$$\beta^{\text{out}}_{\text{read}}(t) = \chi(\beta)\,\mathrm{e}^{-\mathrm{i}\beta\ln\tau\eta}\int_{-\infty}^{\infty}\mathrm{d}\xi\,\mathrm{e}^{\mathrm{i}\xi(\tau-t)}\alpha^{\text{in}}_{\text{read}}(\xi), \tag{92}$$

where we have taken the limits to infinity as the input pulse will be well within the input time and bandwidth of the memory. We can see in this limit the read and write transforms become

true Fourier transforms up to attenuation and phase factors. Indeed, combining these expressions we see that

$$\beta^{\text{out}}_{\text{read}}(t) = 2\pi\,\chi(\beta)^2\,\mathrm{e}^{-\mathrm{i}2\beta\ln\tau\eta}\beta^{\text{in}}_{\text{write}}(t). \tag{93}$$

The total attenuation and phase distortion assuming both long write and broadband assumptions are given by

$$M^{\text{long, broad}}_{\text{write–read}} = 2\pi|\chi(\beta)|^2 = 1-\mathrm{e}^{-2\pi\beta} \tag{94}$$

and

$$\phi^{\text{long, broad}}_{\text{write–read}}(t) = -2\beta\ln\tau\eta. \tag{95}$$

As the phase factor is just a function of system parameters it can be easily cancelled out at the end with a phase plate. Assuming this is implemented we find that the overlap of the input and output pulses of the quantum memory will approach 100% as shown in figure 5(d). In this plot η/σ_η and τ/σ_τ are increased at the same rate and when large enough, all the overlap measures approach the efficiency curve.

4.6. Broadband versus long storage time

Even though their derivations were nearly identical and they were considered as dual approximations, the broadband and long storage time approximations show quite distinct convergences. Indeed, the plots in figure 5 show that the shape overlap in the time domain increases extremely rapidly compared to the frequency domain.

Comparing equations (64) and (69) with (78) and (79), we see that the only important difference between them is the phase distortion factor. While the time has a $(\tau - t)$ factor in both equations frequency has a $(\eta - \xi)$ then $(\eta + \xi)$. If we examine the full transfer from the input field to the output field we get

$$\beta^{\text{out}}_{\text{read}}(t) = \chi^2(\beta)\int_{-\eta}^{\eta}\mathrm{d}\xi\int_{-\tau}^{\tau}\mathrm{d}t'\,\mathrm{e}^{-\mathrm{i}\xi(t'-t)-\mathrm{i}\beta\ln(\tau^2-(t+t')\tau+tt')-\mathrm{i}\beta\ln(\eta^2/4-\xi^2)}\beta^{\text{in}}_{\text{write}}(t). \tag{96}$$

We note that the phase distortion is of a different order in each term. The time factor is of the order ϵ_τ/τ while the frequency one is of the order $(\epsilon_\eta/\eta)^2$. This means that the broad band approximation converges much quicker than the long time approximation.

However this effect can be reduced if the signal is put through the memory twice, a strategy already recognized in [28, 40] as a way to improve the overlap. As we have flipped the transfer functions on the first pass, a second pass will lead to

$$\begin{aligned}\beta^{\text{out}}_{\text{read}}(t) = \chi^4(\beta)\int_{-\eta}^{\eta}\mathrm{d}\xi_1\int_{-\eta}^{\eta}\mathrm{d}\xi_2\int_{-\tau}^{\tau}\mathrm{d}t_1\int_{-\tau}^{\tau}\mathrm{d}t_2\beta^{\text{in}}_{\text{write}}(t_2)\\ \times\mathrm{e}^{-\mathrm{i}\xi_1(t_1-t)-i\xi_2(t_2-t_1)-i\beta\ln(\tau-t_1)^2(\tau+t_2)^2(\eta-\xi_1)^2(\eta+\xi_2)^2},\end{aligned} \tag{97}$$

where now the time and frequency terms are of the same order. We can see the effect that this has on the overlap in figure 6. Here, in contrast to figure 5(d), the overlap, efficiency,TDSO and FDSO all increase at almost the same rate, making the long time and broadband approximations truly equivalent.

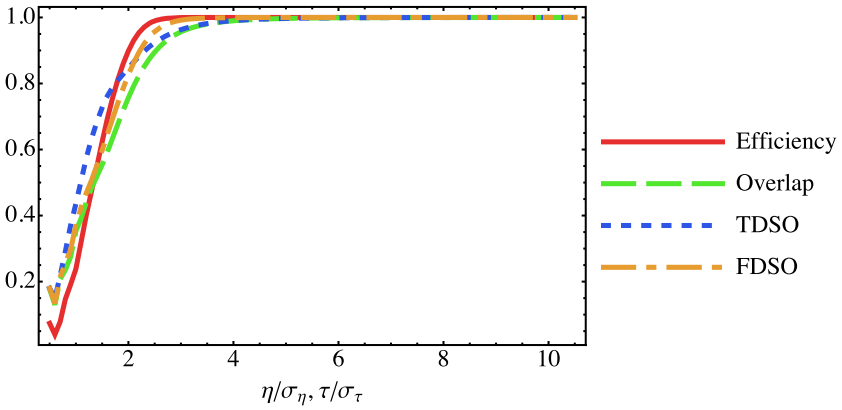

Figure 6. Performance of a double pass through the memory using four different measures: efficiency, overlap, TDSO and FDSO. The data was produced by calculating $\beta^{\text{out}}_{\text{read}}(t)$ using the exact solutions (section 3) twice, with the same parameters as in figure 3, and η/σ_η and τ/σ_τ increasing at the same rate. All the performance measures now improve at the same rate, with the overlap now saturating as quickly as the efficiency. Contrast this to figure 5(d) where the overlap lags behind the efficiency, and there is also an asymmetry between the improvement rate of the TDSO and FDSO.

5. Quantum memory operation: analysis in the frequency domain

The analyses we have used so far to help understand the operation of the GEM have been largely based on time domain studies of the transfer integral operator kernels $h_{\text{write}}(\xi, t)$, $g_{\text{write}}(\xi)$, $h_{\text{read}}(\xi)$ and $g_{\text{read}}(\xi, t)$ governing the write and read stages. While the Fourier transform was used to explain GEM operation using approximations, in this section we complement that analysis by examining further the transfer functions in the Laplace or complex frequency domain. In this manner we are able to plot Bode diagrams for the magnitude and phase of the transfers and thereby gain additional insights into GEM operation by making clear the correlation between the spatial and frequency variables, and by explicitly representing the phase distortion.

The Laplace transform of a function $f(t)$ is defined by

$$\tilde{f}(s) = \int_{0^-}^{t} f(t)\, \mathrm{e}^{-st}\, \mathrm{d}t, \tag{98}$$

where $s = \sigma + \mathrm{i}\omega$ is a complex variable, a generalized frequency. We consider the Laplace transform, and denote by $H_{\text{write}}(\xi, s)$, $G_{\text{write}}(s)$, $H_{\text{read}}(\xi, s)$ and $G_{\text{read}}(\xi, s)$ the Laplace transforms of $h_{\text{write}}(\xi, t)$, $g_{\text{write}}(\xi, t)$, $h_{\text{read}}(\xi, t)$ and $g_{\text{read}}(\xi, t)$ respectively, in the time variable t.

5.1. Write stage

As explained in appendix A.1, the write stage transfer functions in the s-domain are given by

$$H_{\text{write}}(\xi, s) = \frac{\mathrm{i}\sqrt{\beta}}{s + \mathrm{i}\xi} \exp\left(-\beta \int_{-\eta}^{\xi} \frac{\mathrm{d}x}{s + \mathrm{i}x}\right) \tag{99}$$

and

$$G_{\text{write}}(s) = \exp\left(-\beta \int_{-\eta}^{\eta} \frac{\mathrm{d}x}{s + \mathrm{i}x}\right). \tag{100}$$

It is perhaps simplest to start with the transfer function $G_{\text{write}}(s)$, which is responsible for the loss in the write stage and relates the input field to the output field as

$$\tilde{\beta}^{\text{out}}_{\text{write}}(s) = G_{\text{write}}(s)\tilde{\beta}^{\text{in}}_{\text{write}}(s). \tag{101}$$

The time shift does not appear explicitly in equation (101) due to time invariance of the GEM during the write stage (section 3.4).

In engineering and elsewhere, the Bode diagram is a widely used graphical representation of the frequency response of a transfer function. The frequency response concerns the behaviour of $G_{\text{write}}(s)$ when $s = \mathrm{i}\omega$, as ω varies over a range of frequencies. For the transfer function G_{write} we have

$$G_{\text{write}}(\mathrm{i}\omega) = \exp\left(\mathrm{i}\beta \int_{-\eta}^{\eta} \frac{\mathrm{d}x}{\omega + x}\right). \tag{102}$$

The magnitude $M_{G_{\text{write}}}(\mathrm{i}\omega)$ and phase $\phi_{G_{\text{write}}}(\mathrm{i}\omega)$ are defined by

$$G_{\text{write}}(\mathrm{i}\omega) = M_{G_{\text{write}}}(\mathrm{i}\omega)\, \mathrm{e}^{\mathrm{i}\phi_{G_{\text{write}}}(\mathrm{i}\omega)}. \tag{103}$$

These may be evaluated (appendix D) to be

$$M_{G_{\text{write}}}(\mathrm{i}\omega) = \begin{cases} 1 & \text{for } \omega > \eta \text{ or } \omega < -\eta, \\ \exp(-\beta\pi) & \text{for } -\eta < \omega < \eta \end{cases} \tag{104}$$

and

$$\phi_{G_{\text{write}}}(\mathrm{i}\omega) = \beta \ln\left|\frac{\omega + \eta}{\omega - \eta}\right|. \tag{105}$$

The Bode diagram for $G_{\text{write}}(s)$ is shown in figure 7, where the frequency window and phase distortion can clearly be seen. Outside the frequency window, $|\omega| > \eta$, all frequencies pass through. However, within the window, $|\omega| < \eta$, all frequencies are attenuated by a factor $\mathrm{e}^{-\beta\pi}$, consistent with the approximate analysis given in section 4. The attenuated modes must therefore be mostly stored, and may be called *approximate dark states*. Note that for the output light to be nearly dark there must be destructive interference between the internal and incoming contributions, as required by the output equation (8).

We turn now to the transfer function $H_{\text{write}}(\xi, s)$ that relates the input signal to the internal modes

$$\tilde{\alpha}(\xi, s) = H_{\text{write}}(\xi, s)\tilde{\beta}^{\text{in}}_{\text{write}}(s). \tag{106}$$

Here, $\xi \in (-\eta, \eta)$ varies over the spatial range of the GEM. The transfer function $H_{\text{write}}(\xi, s)$ describes how the input is stored at detuning ξ. Evaluating at $s = \mathrm{i}\omega$ we have the frequency response function

$$H_{\text{write}}(\xi, \mathrm{i}\omega) = \frac{\sqrt{\beta}}{\omega + \xi} \exp\left(\mathrm{i}\beta \int_{-\eta}^{\xi} \frac{\mathrm{d}x}{\omega + x}\right) \tag{107}$$

$$= M_{H_{\text{write}}}(\xi, \mathrm{i}\omega)\, \mathrm{e}^{\mathrm{i}\phi_{H_{\text{write}}}(\xi, \mathrm{i}\omega)}, \tag{108}$$

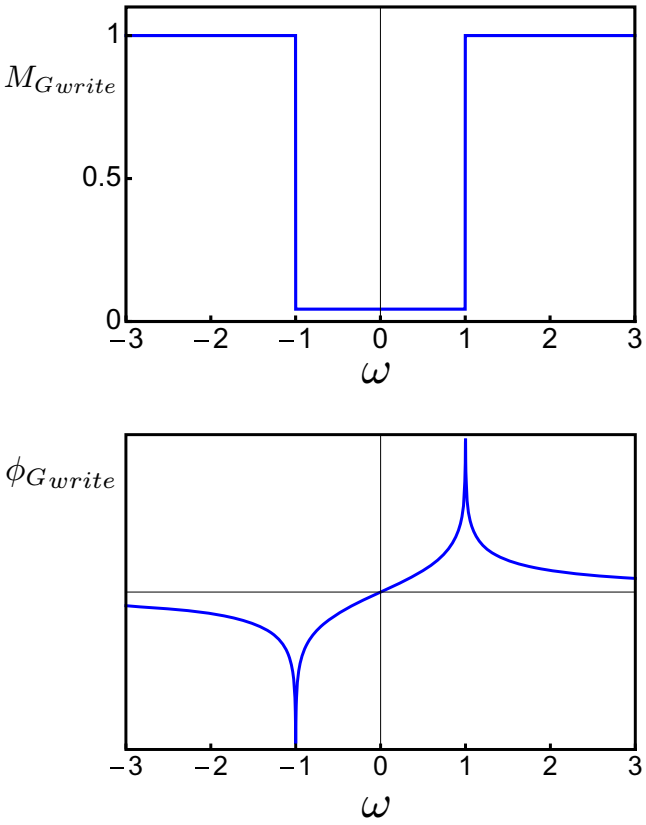

Figure 7. Bode diagram illustrating the frequency response (magnitude $M_{G_{\text{write}}}(\mathrm{i}\omega)$ and phase $\phi_{G_{\text{write}}}(\mathrm{i}\omega)$) for the transfer function $G_{\text{write}}(s)$. The magnitude plot clearly shows the frequency window $-\eta < \xi < \eta$ (with $\eta = 1$ in the plots) within which the incoming modes are absorbed by the memory, and outside of which the modes are passed through. The phase plot shows how the phase of the input is distorted as the signal is either absorbed or passed through.

and the corresponding magnitude and phase are given by

$$M_{H_{\text{write}}}(\xi, \mathrm{i}\omega) = \begin{cases} \dfrac{\sqrt{\beta}}{|\omega+\xi|} & \text{for } \omega > \eta \text{ or } \omega < -\xi \\ \dfrac{\sqrt{\beta}}{|\omega+\xi|}\exp(-\beta\pi) & \text{for } -\xi < \omega < \eta \end{cases} \tag{109}$$

and

$$\phi_{H_{\text{write}}}(\xi, \mathrm{i}\omega) = \begin{cases} \beta \ln|\frac{\omega+\xi}{\omega-\eta}| & \text{for } \omega > -\xi, \\ \pi + \beta \ln|\frac{\omega+\xi}{\omega-\eta}| & \text{for } \omega < -\xi. \end{cases} \tag{110}$$

The Bode diagram for $H_{\text{write}}(\xi, s)$ is shown in figures 8(a) and (b). The plots show the magnitude and phase as a function of the spatial variable ξ and the frequency variable ω. The 'ridge' evident in the magnitude plot shows the correlation $\xi \approx -\omega$ between these variables. The correlation is not perfect, as the ridge has non-zero width, and this is due to the distortions leading to the deviations from the ideal transforms.

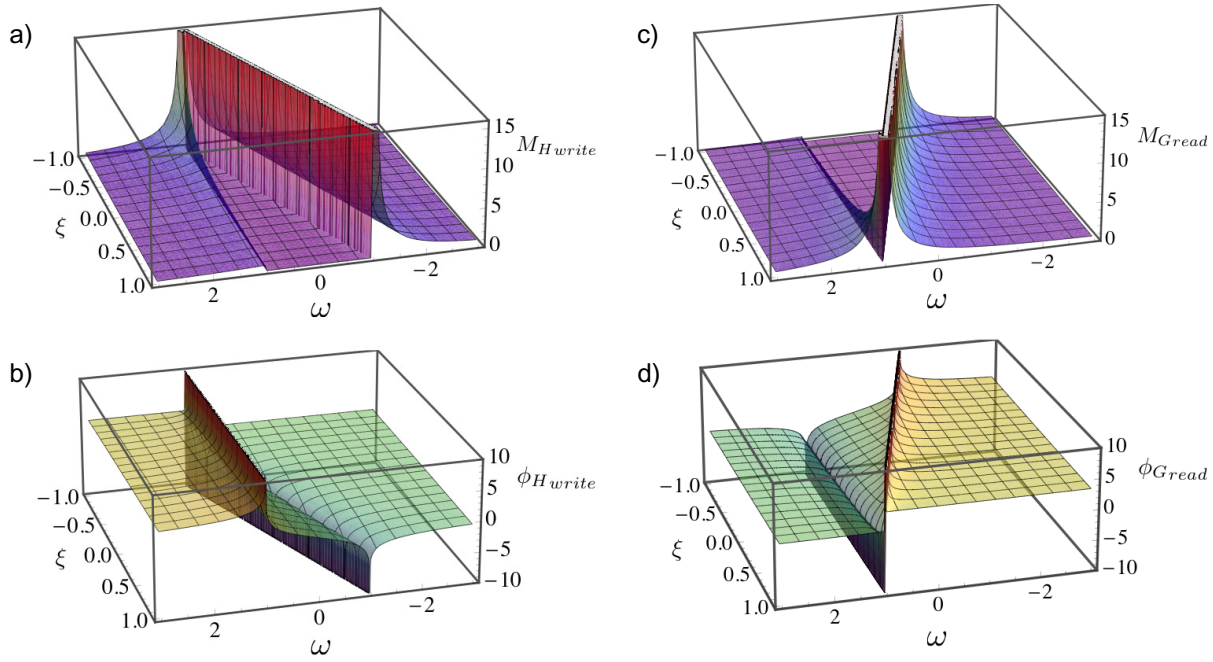

Figure 8. Bode diagram illustrating the frequency response for the transfer functions $H_{\text{write}}(\xi, s)$ (left) and $G_{\text{read}}(\xi, s)$ (right), for the write and read stages, respectively. The plots show the magnitude $M_{H_{\text{write}}}(\xi, \mathrm{i}\omega)$ (a) and phase $\phi_{H_{\text{write}}}(\xi, \mathrm{i}\omega)$ (b) as a function of the spatial variable ξ and the frequency variable ω. On the right, plots (c) and (d) show the corresponding functions for the read phase. In both cases the 'ridges' indicate a correlation between the variables ξ and ω.

With the input expressed in the s-domain, and the internal output in the time domain, we have, using the inverse Laplace transform

$$\alpha^{\text{out}}_{\text{write}}(\xi) = \alpha(\xi, \tau) \tag{111}$$

$$= \frac{1}{2\pi\mathrm{i}} \int_{\sigma-\mathrm{i}\infty}^{\sigma+\mathrm{i}\infty} H_{\text{write}}(\xi, s')\beta^{\text{in}}_{\text{write}}(s')\,\mathrm{e}^{s'\tau}\,\mathrm{d}s' \tag{112}$$

$$= \frac{1}{2\pi\mathrm{i}} \int_{\sigma-\mathrm{i}\infty}^{\sigma+\mathrm{i}\infty} \frac{\mathrm{i}\sqrt{\beta}}{s'+\mathrm{i}\xi} \exp\left(-\beta \int_{-\eta}^{\xi} \frac{\mathrm{d}x}{s'+\mathrm{i}x}\right) \beta^{\text{in}}_{\text{write}}(s')\,\mathrm{e}^{s'\tau}\,\mathrm{d}s', \tag{113}$$

where $-\tau < t < \tau$ is the time interval for the write stage. This expression has the appearance somewhat like a distorted *Hilbert transform* [41]. The ridge suggests that the dominant contributions to this integral will involve $\tilde{\beta}^{\text{in}}_{\text{write}}(-\mathrm{i}\xi)$, consistent with the approximate expression (65). Note that expression (113) depends only on the input signal within the time window $-\tau < t < \tau$ (causality).

5.2. Read stage

The transfer function in the s-domain for internal stored information to the output during the read stage is given by

$$G_{\text{read}}(\xi, s) = \frac{\mathrm{i}\sqrt{\beta}}{s - \mathrm{i}\xi} \exp\left(-\beta \int_{\xi}^{\eta} \frac{\mathrm{d}x}{s - \mathrm{i}x}\right). \tag{114}$$

The frequency response is given by

$$G_{\text{read}}(\xi, \mathrm{i}\omega) = M_{G_{\text{read}}}(\xi, \mathrm{i}\omega)\, \mathrm{e}^{\mathrm{i}\phi_{G_{\text{read}}}(\xi, \mathrm{i}\omega)} \tag{115}$$

and the corresponding magnitude and phase are

$$M_{G_{\text{read}}}(\xi, \mathrm{i}\omega) = \begin{cases} \dfrac{\sqrt{\beta}}{|\omega - \xi|} & \text{for } \omega > \eta \text{ or } \omega < \xi, \\ \dfrac{\sqrt{\beta}}{|\omega - \xi|} \exp(-\beta\pi) & \text{for } \xi < \omega < \eta \end{cases} \tag{116}$$

and

$$\phi_{G_{\text{read}}}(\xi, \mathrm{i}\omega) = \begin{cases} \beta \ln\left|\frac{\omega - \eta}{\omega - \xi}\right| & \text{for } \omega > \xi, \\ \pi + \beta \ln\left|\frac{\omega - \eta}{\omega - \xi}\right| & \text{for } \omega < \xi. \end{cases} \tag{117}$$

The Bode diagram for $G_{\text{read}}(\xi, s)$ is shown in figures 8 (c) and (d). Similar to the write stage, we see a 'ridge' indicating the correlation $\xi \approx \omega$.

The output is given by

$$\tilde{\beta}^{\text{out}}_{\text{read}}(s) = \int_{-\eta}^{\eta} G_{\text{read}}(\xi, -s)\alpha^{\text{in}}_{\text{read}}(\xi)\, \mathrm{d}\xi \tag{118}$$

$$= \int_{-\eta}^{\eta} \frac{-\mathrm{i}\sqrt{\beta}}{s + \mathrm{i}\xi} \exp\left(\beta \int_{\xi}^{\eta} \frac{\mathrm{d}x}{s + \mathrm{i}x}\right) \alpha^{\text{in}}_{\text{read}}(\xi)\, \mathrm{d}\xi. \tag{119}$$

Note that the time shift does not appear explicitly in equation (119) due to time invariance of the GEM during the read stage, and the minus sign in $-s$ is due to the time reversal of the read output (section 3.4). Setting $s = \mathrm{i}\omega$ we have

$$\tilde{\beta}^{\text{out}}_{\text{read}}(\mathrm{i}\omega) = \int_{-\eta}^{\eta} \frac{-\sqrt{\beta}}{\omega + \xi} \exp\left(-\beta \int_{\xi}^{\eta} \frac{\mathrm{d}x}{\omega + x}\right) \alpha^{\text{in}}_{\text{read}}(\xi)\, \mathrm{d}\xi, \tag{120}$$

and we see that the dominant contribution to the integral involves the term $\alpha^{\text{in}}_{\text{read}}(-\mathrm{i}\omega)$. This is consistent with the approximate expression (70). As for the write stage, equation (113), we recognize that the transformation appears somewhat like a distorted Hilbert transform.

6. Conclusions

We have presented and solved analytically a quantum input–output model for GEM which makes no assumptions on the optical depth, memory bandwidth or storage times. The model was shown to be equivalent to previous model of memories in the weak atomic excitation regime and we demonstrated that our general solution reduces to previous results in the appropriate limits.

Using this solution we investigated the memory fidelity in the regime of high optical depth and finite bandwidth that maximizes efficiency in experiments. We obtained general expressions for several measures of storage quality due to the nonlinear phase-shifts that occur when optical depth is high. We also confirmed that storing a pulse twice may be used to largely undo this shift.

The presented solution will be helpful as-is to understand and optimize high efficiency memory experiments in the weak atomic excitation regime. The nonlinear phase-shift investigated here has previously been identified as a major limiting factor for the practical use of GEM [31]. Accurate predictions of this shift should aid general correction or accounting for it. In the long term, our model is a starting point to investigate the designing of complex networks containing GEM.

The presented solution should serve also as a building block to describing more complex behaviour. It has previously been shown that manipulating the detuning gradient during the output stage can be used to modify the output pulse [42]. Going further than this, by incorporating a general detuning function (dependent on time and space) beyond a simple gradient, it should be possible to model general transformations on a light pulse, including correcting the nonlinear phase-shift using no external components. This would be experimentally realizable by using complex electrode or solenoid arrangements. In this respect, our analysis in terms of transfer functions is also helpful as it establishes a strong connection with signal processing theory and, with it, the possibility of using the plethora of methods in the field to manipulate the input signal via GEM. It is hoped that our approach will be accessible to those in the signal processing field. Finally, as the model fully accounts for quantum mechanics it will be useful for describing conditional measurements and storage of non-classical states.

Acknowledgments

We thank P K Lam, B Buchler, M Hosseini, M Sellars, K Ferguson and N Yamamoto for useful discussions. We gratefully acknowledge support by the Australian Research Council Centre of Excellence for Quantum Computation and Communication Technology (project number CE110001027) and the Air Force Office of Scientific Research (grant numbers FA2386-09-1-4089 and FA2386-12-1-4075).

Appendix A. Deriving the analytic solution

In this appendix we derive four transfer functions of the following equations:

$$\partial_t \alpha(\xi, t) = \mp \mathrm{i}\xi\alpha(\xi, t) + \mathrm{i}\sqrt{\beta}\beta(\xi, t), \tag{A.1}$$

$$\partial_\xi \beta(\xi, t) = \mathrm{i}\sqrt{\beta}\alpha(\xi, t), \tag{A.2}$$

which are a repeat of equations (27) and (28). We can solve these equations using a variation of a parameters method. These solutions can then be used to uniquely identify the transfer functions in the time domain. We could have directly found the transfer functions from their LTI form, however that involves the exponentiation of an infinite dimensional matrix which can get rather technical.

We will solve the system during a write then read phase each of which will go for a time period of T. During the write phase we set the gradient to be positive while during the read phase we set it to be negative.

A.1. Write phase

During the write phase we will assume there is no excitation in the atoms initially, thus we can set $\alpha(\xi, 0) = 0$, although the operator is non zero, any expectation value taken will be zero, so this it is sufficient to simply apply this.

We take the Laplace transform, as defined in equation (98), of (A.1) with regard the time variable to find

$$s\tilde{\alpha}(\xi, s) = -\mathrm{i}\xi\,\tilde{\alpha}(\xi, s) + \mathrm{i}\sqrt{\beta}\,\tilde{\beta}(\xi, s), \tag{A.3}$$

where we have set $\tilde{\alpha}(\xi, 0) = 0$ during the write phase. We can rearrange (A.3) to find

$$\tilde{\alpha}(\xi, s) = \frac{\mathrm{i}\sqrt{\beta}}{s + \mathrm{i}\xi}\tilde{\beta}(\xi, s). \tag{A.4}$$

Replacing equation (A.4) into (A.2)

$$\partial_\xi \tilde{\beta}(\xi, s) = \frac{-\beta}{s + \mathrm{i}\xi}\tilde{\beta}(\xi, s). \tag{A.5}$$

We can solve equation (A.4) to find

$$\begin{aligned}\tilde{\beta}(\xi, s) &= \exp\left(\int_{-\eta}^{\xi} \mathrm{d}\xi' \frac{-\beta}{s + \mathrm{i}\xi'}\right)\tilde{\beta}(-\eta, s)\\ &= \left(\frac{s + \mathrm{i}\xi}{s - \mathrm{i}\eta}\right)^{\mathrm{i}\beta}\tilde{\beta}(-\eta, s).\end{aligned} \tag{A.6}$$

Lastly we can use a mathematical package such as *Mathematica* [43] and transform back to real time to find

$$\beta(\xi, t) = \int_0^t \mathrm{d}t'\Big(-(\eta + \xi)\beta\,\mathrm{e}^{-\mathrm{i}\xi(t-t')}\,{}_1F_1\left(1 + \mathrm{i}\beta, 2, \mathrm{i}(\xi + \eta)(t - t')\right) + \delta(t - t')\Big)\beta(-\eta, t'). \tag{A.7}$$

This is our first solution for equations (A.1) and (A.2). Equation (A.7) gives us the evolution of the outgoing light field during the write stage. In the main text this solution is presented as a transfer function in equation (31) where we define $\beta^{\mathrm{out}}_{\mathrm{write}}(t) = \beta(\eta, t)$ and $\beta^{\mathrm{in}}_{\mathrm{write}}(t) = \beta(-\eta, t')$.

We can also find what quantum information is transferred on to the atoms. Replacing (A.6) into (A.4) we find

$$\tilde{\alpha}(\xi, s) = \frac{\mathrm{i}\sqrt{\beta}}{s + \mathrm{i}\xi}\left(\frac{s + \mathrm{i}\xi}{s - \mathrm{i}\eta}\right)^{\mathrm{i}\beta}\tilde{\beta}(-\eta, s). \tag{A.8}$$

We can transform equation (A.8) back into the time domain and find

$$\alpha(\xi, t) = \int_0^t \mathrm{d}t' i\sqrt{\beta}\,\mathrm{e}^{-\mathrm{i}\xi(t-t')}L\left(-\mathrm{i}\beta, \mathrm{i}(t - t')(\xi + \eta)\right)\beta(-\eta, t'). \tag{A.9}$$

This is our second solution. Equation (A.9) gives us the final quantum state of the atoms after the write stage. In the main text this solution is presented as a transfer function in equation (30) where we define $\alpha^{\mathrm{out}}_{\mathrm{write}}(\xi) = \alpha(\xi, T)$.

A.2. Read phase

During the read phase we assume there is no light coming into the system so we set $\beta(-\eta, t) = 0$. However, now we can no longer assume that there is no excitation left in the material so we have $\alpha^{\text{in}}_{\text{read}}(\xi) = \alpha(\xi, T)$. We again solve (A.1) and (A.2) with this boundary condition and a change on the sign of the gradient.

Taking the Laplace transform of (A.1) and taking to account our changed boundary conditions we find

$$s\tilde{\alpha}(\xi, s) - \alpha(\xi, T) = \mathrm{i}\xi\tilde{\alpha}(\xi, s) + \mathrm{i}\sqrt{\beta}\tilde{\beta}(\xi, s). \tag{A.10}$$

We can rearrange (A.10) to get

$$\tilde{\alpha}(\xi, s) = \frac{\alpha(\xi, T)}{s - \mathrm{i}\xi} + \frac{\mathrm{i}\sqrt{\beta}}{s - \mathrm{i}\xi}\tilde{\beta}(\xi, s). \tag{A.11}$$

Replacing (A.11) into (A.2) we find

$$\partial_\xi\tilde{\beta}(\xi, s) = \frac{\mathrm{i}\sqrt{\beta}\alpha(\xi, T)}{s - \mathrm{i}\xi} - \frac{\beta}{s - \mathrm{i}\xi}\tilde{\beta}(\xi, s). \tag{A.12}$$

Equation (A.12) is an inhomogeneous differential equation which we can solve to get

$$\begin{aligned}\tilde{\beta}(\xi, s) &= \int_{-\eta}^{\xi} \mathrm{d}\xi' \frac{\mathrm{i}\sqrt{\beta}}{s - \mathrm{i}\xi'} \exp\left(\int_{\xi'}^{\xi} \mathrm{d}\xi'' \frac{-\beta}{s - \mathrm{i}\xi''}\right) \alpha(\xi', T) \\ &= \int_{-\eta}^{\xi} \mathrm{d}\xi' \frac{\mathrm{i}\sqrt{\beta}}{s - \mathrm{i}\xi'} \left(\frac{s - \mathrm{i}\xi'}{s - \mathrm{i}\xi}\right)^{\mathrm{i}\beta} \alpha(\xi', T).\end{aligned} \tag{A.13}$$

Where we assumed $\beta(-\eta, s) = 0$. We can change equation (A.13) to the time domain to get the solution

$$\beta(\xi, t) = \int_{-\eta}^{\xi} \mathrm{d}\xi' \mathrm{i}\sqrt{\beta}\, \mathrm{e}^{\mathrm{i}\xi' t} L\left(-\mathrm{i}\beta, \mathrm{i}t(\xi - \xi')\right) \alpha(\xi', T). \tag{A.14}$$

This is the third solution. Equation (A.14) gives us the evolution of the outgoing light field during the read stage. In the main text it is presented as a transfer function in equation (35) where $\beta^{\text{out}}_{\text{read}}(t) = \tilde{\beta}(\eta, t)$ and $\alpha^{\text{in}}_{\text{read}}(\xi) = \alpha(\xi', T)$.

Finally we can find the total excitation left in the atoms by replacing (A.13) into (A.11) to find

$$\tilde{\alpha}(\xi, s) = \frac{1}{s - \mathrm{i}\xi} \int_{-\eta}^{\xi} \mathrm{d}\xi' \left(\delta(\xi - \xi') + \frac{-\beta}{s - \mathrm{i}\xi'} \left(\frac{s - \mathrm{i}\xi'}{s - \mathrm{i}\xi}\right)^{i\beta} \alpha(\xi', T)\right). \tag{A.15}$$

We can equation (A.15) into the time domain to get

$$\begin{aligned}\alpha(\xi, t) = \int_{-\eta}^{\xi} \mathrm{d}\xi' \Big(&\delta(\xi - \xi') - (t - T)\beta\, \mathrm{e}^{-\mathrm{i}(\xi - \xi')(t - T)} \\ &\times {}_1F_1\left(1 + \mathrm{i}\beta, 2, \mathrm{i}(t - T)(\xi - \xi')\right)\Big)\alpha(\xi', T).\end{aligned} \tag{A.16}$$

This is the fourth and final solution. Equation (A.16) gives the final quantum state of the atoms after the read stage. In the main text is presented as a transfer function in equation (34) where $\alpha^{\text{out}}_{\text{read}}(\xi) = \alpha(\xi, 2T)$.

Appendix B. Analytic functions

Two analytic functions form part of the analytic solution presented in this paper which are not commonly seen. We provide their definition in terms of power series for the interested reader, in practice they can be calculated efficiently using mathematical packages such as *Mathematica* [43]. We define first the Kummer confluent hypergeometric function [44]

$$ {}_1F_1(a,b,x) = \sum_{k=0}^{\infty} \frac{a^{(n)} z^n}{b^{(n)} n!}, \tag{B.1}$$

where $a^{(n)} = a(a+1)(a+2)\cdots(a+n-1)$. This first arises while deriving the analytic solution in equation (A.7) and is repeated in the main text in equation (32*b*). The other important function is Laguerre function, which we define in terms of the Kummer confluent hypergeometric as

$$ L(n,x) = \frac{{}_1F_1(-n,1,x)}{\Gamma(n+1)}, \tag{B.2}$$

where $\Gamma(n+1)$ is the Gamma function. This first arises when deriving the analytic solution in equation (A.9) and is repeated in the main text in equation (32*a*). When n is integer and x is real this power series generates the well known Laguerre polynomials, however in this paper both n and x are always purely imaginary.

Appendix C. Complex Laguerre function approximation

The transformation kernel for writing the quantum information of the light onto the atomic states (and vice versa) is difficult to analyse in its exact form. Both the write and read transfer functions, equations (32*a*) and (39) respectively, contain complex Laguerre functions of the following form $L(-\mathrm{i}\beta, \mathrm{i}(\tau - t)(\eta \pm \xi))$. Fortunately the form of these kernels simplifies significantly in the physically relevant limit of the total time stored or the bandwidth being large. More precisely if we define $1/x = (\tau - t)(\eta \pm \xi)$, we find the Taylor expansion of $L(-\mathrm{i}\beta, \mathrm{i}/x)$ for $|x| \ll 1$ is

$$ L(-\mathrm{i}\beta, \mathrm{i}/x) \approx \frac{\mathrm{e}^{-\pi\beta/2} x^{\mathrm{i}\beta}}{\Gamma(1-\mathrm{i}\beta)} + O(|x|). \tag{C.1}$$

Truncating to zeroth order and replacing in our definition for x we find

$$ L(-\mathrm{i}\beta, \mathrm{i}(\tau - t)(\eta \pm \xi)) \approx \frac{\mathrm{e}^{-\pi\beta/2 - \mathrm{i}\beta \ln(\tau - t)(\eta \pm \xi)}}{\Gamma(1-\mathrm{i}\beta)}. \tag{C.2}$$

This can be replaced into equations (32*a*) and (39) to get a much simpler transformation kernel. This form makes salient what the memories efficiency is and where the phase distortion comes from.

Appendix D. Magnitude and phase evaluation

Some care is required in evaluation of the magnitude and phase of the transfer functions, since improper integrals and complex logarithms are involved.

We use a branch of the complex logarithm that includes the negative real line, so that, for example, $\ln(-1) = \mathrm{i}\pi$. The reason for this is that if we carry out the integration in (102)

we obtain formally $\mathrm{Log}(\frac{\omega+\eta}{\omega-\eta})$, and the ratio $\frac{\omega+\eta}{\omega-\eta}$ is negative in the range $-\eta < \omega < \eta$. So $\mathrm{Log}(\frac{\omega+\eta}{\omega-\eta}) = \ln|\frac{\omega+\eta}{\omega-\eta}| + \mathrm{i}\pi$ for $-\eta < \omega < \eta$. The magnitude and phase may also be evaluated alternatively by an approximation involving $\sigma + \mathrm{i}\omega$ with σ small and positive.

The attenuation is rather interesting, since each oscillator G_k in the approximating network of section 2 is *all pass*, meaning $|G_k(\mathrm{i}\omega) = 1$ for all ω. What is happening is that the poles of each cavity, which have strictly negative real parts, are moving in the limit to the imaginary axis, resulting in a transfer function with a continuum of purely imaginary poles.

References

[1] Lvovsky A I, Sanders B C and Tittel W 2009 Optical quantum memory *Nature Photon.* **3** 706–14

[2] Walls D F and Milburn G J 1994 *Quantum Optics* (Berlin: Springer)

[3] Boller K J, Imamolu A and Harris S E 1991 Observation of electromagnetically induced transparency *Phys. Rev. Lett.* **66** 2593

[4] Kraus B, Tittel W, Gisin N, Nilsson M, Kröll S and Cirac J I 2006 Quantum memory for nonstationary light fields based on controlled reversible inhomogeneous broadening *Phys. Rev.* A **73** 020302

[5] Alexander A L, Longdell J J, Sellars M J and Manson N B 2006 Photon echoes produced by switching electric fields *Phys. Rev. Lett.* **96** 043602

[6] Hétet G, Longdell J J, Alexander A L, Lam P K and Sellars M J 2008 Electro-optic quantum memory for light using two-level atoms *Phys. Rev. Lett.* **100** 023601

[7] Afzelius M, Simon C, de Riedmatten H and Gisin N 2009 Multimode quantum memory based on atomic frequency combs *Phys. Rev.* A **79** 052329

[8] McAuslan D L, Ledingham P M, Naylor W R, Beavan S, Hedges M P, Sellars M J and Longdell J J 2011 Photon-echo quantum memories in inhomogeneously broadened two-level atoms *Phys. Rev.* A **84** 1–7

[9] Damon V, Bonarota M, Louchet-Chauvet A, Chanelière T and Le Gouët J-L 2011 Revival of silenced echo and quantum memory for light *New J. Phys.* **13** 093031

[10] Moiseev S A and Tittel W 2011 Optical quantum memory with generalized time-reversible atom–light interaction *New J. Phys.* **13** 063035

[11] Duan L M, Lukin M D, Cirac J I and Zoller P 2001 Long-distance quantum communication with atomic ensembles and linear optics *Nature* **414** 413–8

[12] Ledingham P M, Naylor W R and Longdell J J 2010 Nonclassical photon streams using rephased amplified spontaneous emission *Phys. Rev.* A **81** 012301

[13] Chanelière T, Matsukevich D N, Jenkins S D, Lan S-Y, Kennedy T A B and Kuzmich A 2005 Storage and retrieval of single photons transmitted between remote quantum memories *Nature* **438** 833–6

[14] Eisaman M D, André A, Massou F, Fleischhauer M, Zibrov A S and Lukin M D 2005 Electromagnetically induced transparency with tunable single-photon pulses *Nature* **438** 837–41

[15] Appel J, Figueroa E, Korystov D, Lobino M and Lvovsky A I 2008 Quantum memory for squeezed light *Phys. Rev. Lett.* **100** 093602

[16] Choi K S, Deng H, Laurat J and Kimble H J 2008 Mapping photonic entanglement into and out of a quantum memory *Nature* **452** 67

[17] Honda K, Akamatsu D, Arikawa M, Yokoi Y, Akiba K, Nagatsuka S, Tanimura T, Furusawa A and Kozuma M 2008 Storage and retrieval of a squeezed vacuum *Phys. Rev. Lett.* **100** 093601

[18] Longdell J J, Fraval E, Sellars M J and Manson N B 2005 Stopped light with storage times greater than one second using electromagnetically induced transparency in a solid *Phys. Rev. Lett.* **95** 063601

[19] Hedges M P, Longdell J J, Li Y and Sellars M J 2010 Efficient quantum memory for light *Nature* **465** 1052–6

[20] Hosseini M, Sparkes B M, Campbell G, Lam P K and Buchler B C 2011 High efficiency coherent optical memory with warm rubidium vapour *Nature Commun.* **2** 174

[21] Hosseini M, Campbell G, Sparkes B M, Lam P K and Buchler B C 2011 Unconditional room-temperature quantum memory *Nature Phys.* **7** 794–8
[22] Clausen C, Usmani I, Bussieres F, Sangouard N, Afzelius M, de Riedmatten H and Gisin N 2011 Quantum storage of photonic entanglement in a crystal *Nature* **469** 508–11
[23] Saglamyurek E, Sinclair N, Jin J, Slater J A, Oblak D, Bussieres F, George M, Ricken R, Sohler W and Tittel W 2011 Broadband waveguide quantum memory for entangled photons *Nature* **469** 512–5
[24] Radnaev A G, Dudin Y O, Zhao R, Jen H H, Jenkins S D, Kuzmich A and Kennedy T A B 2010 A quantum memory with telecom-wavelength conversion *Nature Phys.* **6** 894–9
[25] Alexander A L 2007 Investigation of quantum information storage in rare earth doped materials *PhD Thesis* Australian National University
[26] Hétet G, Hosseini M, Sparkes B M, Oblak D, Lam P K and Buchler B C 2008 Photon echoes generated by reversing magnetic field gradients in a rubidium vapor *Opt. Lett.* **33** 2323–5
[27] Hosseini M, Sparkes B M, Hetet G, Longdell J J, Lam P K and Buchler B C 2009 Coherent optical pulse sequencer for quantum applications *Nature* **461** 241–5
[28] Longdell J J, Hétet G, Lam P K and Sellars M J 2008 Analytic treatment of controlled reversible inhomogeneous broadening quantum memories for light using two-level atoms *Phys. Rev.* A **78** 032337
[29] Hétet G, Longdell J J, Sellars M J, Lam P K and Buchler B C 2008 Multimodal properties and dynamics of gradient echo quantum memory *Phys. Rev. Lett.* **101** 203601
[30] Nunn J, Reim K, Lee K C, Lorenz V O, Sussman B J, Walmsley I A and Jaksch D 2008 Multimode memories in atomic ensembles *Phys. Rev. Lett.* **101** 260502
[31] Moiseev S A and Arslanov N M 2008 Efficiency and fidelity of photon-echo quantum memory in an atomic system with longitudinal inhomogeneous broadening *Phys. Rev.* A **78** 023803
[32] Gardiner C W and Zoller P 2004 *Quantum Noise* 3rd edn (Berlin: Springer)
[33] Gardiner C W 1993 Driving a quantum system with the output field from another driven quantum system *Phys. Rev. Lett.* **70** 2269–72
[34] Carmichael H J 1993 Quantum trajectory theory for cascaded open systems *Phys. Rev. Lett.* **70** 2273–6
[35] Gough J and James M R 2009 The series product and its application to quantum feedforward and feedback networks *Autom. Control IEEE Trans.* **54** 2530–44
[36] Protsenko I, Domokos P, Lefèvre-Seguin V, Hare J, Raimond J M and Davidovich L 1999 Quantum theory of a thresholdless laser *Phys. Rev.* A **59** 1667–82
[37] Carmichael H J 1993 *An Open Systems Approach to Quantum Optics* (Berlin: Springer)
[38] Kailath T 1980 *Linear Systems* (Englewood Cliffs, NJ: Prentice-Hall)
[39] Bouten L, Van Handel R and James M 2007 An introduction to quantum filtering *SIAM J. Control Optim.* **46** 2199–241
[40] Hétet G 2008 Quantum memories for continuous variable states of light in atomic ensembles *PhD Thesis* Australian National University Canberra
[41] Bracewell R N 1986 *The Fourier Transform and its Applications* 2nd edn (New York: McGraw-Hill)
[42] Buchler B C, Hosseini M, Hétet G, Sparkes B M and Lam P K 2010 Precision spectral manipulation of optical pulses using a coherent photon echo memory *Opt. Lett.* **35** 1091–3
[43] (Wolfram Research) 2012 *Mathematica* version 9.0 ed (Champaign, IL: Wolfram Research, Inc.)
[44] Abramowitz M and Stegun I A (ed) 1972 *Handbook of Mathematical Functions with Formulas, Graphs and Mathematical Tables* 10th printing edn (Washington, DC: Department of Commerce United States of America) p 504